AEDC-TR-78-60

CALIBRATION OF THE AEDC-PWT 16-FT TRANSONIC TUNNEL AERODYNAMIC TEST SECTION AT VARIOUS REYNOLDS NUMBERS

F. M. Jackson III
ARO, Inc., a Sverdrup Corporation Company

PROPULSION WIND TUNNEL FACILITY
ARNOLD ENGINEERING DEVELOPMENT CENTER
AIR FORCE SYSTEMS COMMAND
ARNOLD AIR FORCE STATION, TENNESSEE 37389

February 1979

Final Report for Period April 1976 — June 1978

Approved for public release; distribution unlimited.

Prepared for

ARNOLD ENGINEERING DEVELOPMENT CENTER/DOTR
ARNOLD AIR FORCE STATION, TENNESSEE 37389

This report has been reviewed by the Information Office (OI) and is releasable to the National Technical Information Service (NTIS). At NTIS, it will be available to the general public, including foreign nations.

APPROVAL STATEMENT

This report has been reviewed and approved.

JAMES M. McGEE, 2d Lt, USAF
Test Director, PWT Division
Directorate of Test Operations

Approved for publication:

FOR THE COMMANDER

JAMES D. SANDERS, Colonel, USAF
Director of Test Operations
Deputy for Operations

UNCLASSIFIED

REPORT DOCUMENTATION PAGE		READ INSTRUCTIONS BEFORE COMPLETING FORM
1 REPORT NUMBER AEDC-TR-78-60	2 GOVT ACCESSION NO.	3 RECIPIENT'S CATALOG NUMBER
4 TITLE (and Subtitle) CALIBRATION OF THE AEDC-PWT 16-FT TRANSONIC TUNNEL AERODYNAMIC TEST SECTION AT VARIOUS REYNOLDS NUMBERS		5 TYPE OF REPORT & PERIOD COVERED Final Report, April 1976 – June 1978
		6 PERFORMING ORG REPORT NUMBER
7 AUTHOR(s) F. M. Jackson III, ARO, Inc., a Sverdrup Corporation Company		8 CONTRACT OR GRANT NUMBER(s)
9 PERFORMING ORGANIZATION NAME AND ADDRESS Arnold Engineering Development Center Air Force Systems Command Arnold Air Force Station, Tennessee 37389		10 PROGRAM ELEMENT, PROJECT, TASK AREA & WORK UNIT NUMBERS Program Element 65807F
11 CONTROLLING OFFICE NAME AND ADDRESS Arnold Engineering Development Center/OIS Air Force Systems Command Arnold Air Force Station, Tennessee 37389		12 REPORT DATE February 1979
		13 NUMBER OF PAGES 177
14 MONITORING AGENCY NAME & ADDRESS(If different from Controlling Office)		15 SECURITY CLASS (of this report) UNCLASSIFIED
		15a. DECLASSIFICATION DOWNGRADING SCHEDULE N/A

16 DISTRIBUTION STATEMENT (of this Report)

Approved for public release; distribution unlimited.

17 DISTRIBUTION STATEMENT (of the abstract entered in Block 20, if different from Report)

Available in DDC.

18 SUPPLEMENTARY NOTES

19 KEY WORDS (Continue on reverse side if necessary and identify by block number)

calibration   AEDC-PWT-16T
interference
transonic wind tunnels
walls
Mach number

20 ABSTRACT (Continue on reverse side if necessary and identify by block number)

Tests were conducted in the AEDC Propulsion Wind Tunnel (16T) to determine the tunnel test section Mach number distributions and calibration at various Reynolds numbers. Two separate test entries were made. Collectively, the calibration was conducted at Mach numbers from 0.2 to 1.6 and at Reynolds numbers from 0.5×10^6/ft to 6.0×10^6/ft. The calibration was conducted with the aerodynamic test section (Test Section 2) using a centerline pipe

DD FORM 1473 1 JAN 73   EDITION OF 1 NOV 65 IS OBSOLETE

UNCLASSIFIED

20.   ABSTRACT (Continued)

and/or wall pressure orifices to define the Mach number distributions. A quantitative evaluation of the effects of tunnel pressure ratio, test section wall angle, and Reynolds number on the tunnel Mach number distributions and calibration was accomplished. The results indicate that good quality Mach number distributions are obtained for both zero and the optimum wall angle schedule. To obtain the maximum accuracy, the Tunnel 16T calibration must be defined as a function of test section wall angle, Reynolds number, and Mach number. Comparison of this calibration with previous calibration results indicates that a revision in the tunnel calibration utilized for operations is desirable. Analytical expressions which represent the tunnel calibration at various test conditions were developed for utilization during Tunnel 16T operations.

AFSC
Arnold AFS Tenn

PREFACE

The work reported herein was conducted by the Arnold Engineering Development Center (AEDC), Air Force Systems Command (AFSC), at the request of the AEDC Test and Technology Divisions. The Air Force project managers were Mr. E. R. Thompson and Lt. Colonel J. C. Cardosi. The results of the test were obtained by ARO, Inc., AEDC Division (a Sverdrup Corporation Company), operating contractor for the AEDC, AFSC, Arnold Air Force Station, Tennessee, under ARO Project Numbers P32A-G1A, P41T-G1A, and P41T-L0B. The manuscript was submitted for publication on September 1, 1978.

CONTENTS

ILLUSTRATIONS

APPENDIX

1.0 INTRODUCTION

The AEDC Propulsion Wind Tunnel (16T) was put into operation in July 1956. Initially, tunnel calibrations were conducted for the two test sections (aerodynamic and propulsion) available for tests. Subsequently, tunnel or equipment modification, the resolution of the effect of some tunnel parameter, or the need for improved data quality precipitated several additional tunnel calibrations. Collectively, the early calibration work revealed that (within the existing data accuracy). 1) the calibrations for the aerodynamic and propulsion test sections were the same. 2) the tunnel calibration could be based on use either of wall orifices or of a centerline pipe, 3) stagnation pressure variation did not have a significant effect upon the tunnel calibration, 4) tunnel pressure ratio variation did not normally have a significant effect upon the tunnel calibration, and 5) test section wall angle variation had a significant effect upon the tunnel calibration.

In 1965, following the installation of fiberglass compressor blades in Tunnel 16T, a calibration was conducted with the aerodynamic test section. This calibration (Ref. 1) was based on pressure orifices located in a 2-ft-wide solid plate in the test section floor. The Ref. 1 calibration remained in use in Tunnel 16T until May 1977.

The determination of engine inlet and nozzle performance is an integral part of the development program for modern weapon systems. In recent years several wind tunnel tests have been conducted at AEDC to determine nozzle afterbody pressure drag for various systems. A comprehensive program was also conducted at AEDC to investigate various aspects of problems associated with integrated nozzle/afterbody (NAB) testing in the transonic flow regime. A particular objective of this program was to evaluate the effect of Reynolds number on nozzle afterbody pressure drag.

To support the program for improving NAB test techniques, tests were conducted in the propulsion test section of Tunnel 16T to determine the tunnel calibration and centerline Mach number distributions at various test section wall porosities and Reynolds numbers. During the porosity calibration (Ref. 2), limited data obtained at $M_\infty = 0.6$ and 0.8 indicated that the calibrated Mach number increased slightly (less than 0.001 per million) with increasing Reynolds number. For 6 percent porosity and at all Reynolds numbers, however, the Ref. 2 calibrated Mach number agreed within ±0.002 with the calibration reported in Ref. 1.

Following the calibration reported in Ref. 2, an analysis of the effects of variation of the tunnel calibration with Reynolds number on NAB test data was conducted. This analysis revealed that a 0.2-percent error in static pressure attributed to use of the Ref. 1

calibration, which neglects the effects of Reynolds number, could cause a 70 drag count (based on maximum model cross-sectional area) error in nozzle afterbody drag at M_∞ = 0.6 and Re = 5.0 x 10^6/ft. As a consequence of these results, a test was conducted to completely define the effects of Reynolds number variation on the Tunnel 16T calibration. The results of this calibration, which was conducted with the propulsion test section, are presented in Ref. 3. The results of the Refs. 2 and 3 calibrations were incorporated into appropriate computer programs for utilization during Tunnel 16T operation and for correction of some AEDC NAB test data.

Considering the sensitivity of nozzle afterbody data to small changes in the tunnel calibration, the adequacy of using the same tunnel calibration for both the aerodynamic and propulsion test sections came into question. Data obtained parasitically during a NAB test in the aerodynamic test section indicated that the effects of Reynolds number on the tunnel calibration were more pronounced in the aerodynamic test section than in the propulsion test section. These results precipitated two calibration entries in the aerodynamic test section. The first calibration entry, which was limited in scope and based on wall pressure measurements, confirmed that the aerodynamic and propulsion test sections had different Reynolds number effects. As a consequence, a second calibration entry was made to completely define the effects of Reynolds number variation on the Tunnel 16T calibration with the aerodynamic test section. This latter calibration entry utilized both wall and centerline pipe pressures.

The results of the Reynolds number calibrations in the aerodynamic test section are presented in this report. During these calibrations, centerline Mach number distributions were obtained at Mach numbers from 0.2 to 1.6 and for Reynolds numbers from about 0.5 to 6.0 x 10^6/ft. The effects of tunnel pressure ratio and test section wall angle on the tunnel calibration and power consumption were also determined. The results of these calibrations have been utilized to correct data for AEDC NAB tests conducted in the aerodynamic test section. The results of the calibrations have also been incorporated into a computer program for utilization during Tunnel 16T operations.

2.0 APPARATUS

2.1 TEST FACILITY

The AEDC Propulsion Wind Tunnel Facility (PWT) 16-ft Transonic Wind Tunnel [Propulsion Wind Tunnel (16T)] is a continuous flow, closed-circuit tunnel which can be operated at Mach numbers from 0.2 to 1.6. The maximum attainable Mach number can vary slightly, depending upon the tunnel pressure ratio requirements with a particular test

installation. Tunnel 16T is a variable density tunnel which can be operated with a stagnation pressure range from 120 to 4,000 psfa. The maximum attainable pressure is a function of Mach number and the availability of electrical power. The tunnel stagnation temperature can be varied from a minimum of about 80°F, dependent upon available cooling water temperature, to a maximum of 160°F.

Tunnel 16T has a test section 40 ft long and 16 ft square with 6-percent porosity walls. The general arrangement of the test section and the perforated wall geometry is shown in Fig. 1. The test section sidewalls can be either converged or diverged 1 deg. Two test sections are available for testing in Tunnel 16T. Test Section 1 is generally used for propulsion testing. Test Section 2. which is equipped with a sting support system, is used primarily for aerodynamic testing. The calibration reported herein utilized the aerodynamic test section.

The Tunnel 16T main compressor is a three-stage, axial-flow compressor with variable stator blades. The compressor drive system consists of four motors with a power rating of 216,000 hp. To prevent tunnel choking in the transonic Mach number range, test section flow removal (auxiliary flow) is accomplished with a plenum evacuation system (PES). The PES consists of ten compressors which are driven by motors with a total power rating of 179,000 hp. The PES is also utilized to control tunnel pressure level.

Various Mach numbers in Tunnel 16T are established by regulation of pressure ratio, plenum pressure, and the contour of a flexible, two-dimensional Laval nozzle. Mach numbers below 0.55 are obtained by operating the compressor drive motors subsynchronously. Test section flow removal is required at $M_\infty > 0.75$, and supersonic nozzle contours are utilized at $M_\infty \geqslant 1.05$. Additional details concerning Tunnel 16T and its capabilities are presented in Ref. 4.

2.2 CALIBRATION EQUIPMENT

For test entry 2. a 6.5-in.-diam static pressure pipe was used to obtain the centerline static pressure distribution from tunnel station -5.9 to 24.1. The rear end of the calibration pipe was attached to the tunnel sting support system. A mechanism was provided to counteract pipe sway and sag. Four cables, swept rearward at 30 deg to the tunnel centerline and spaced to produce a moment to also aid in removing pipe sag, provided pipe support. The pipe. which had an ogive tip. was subject to a tensile load through the use of a cable which extended far upstream into the tunnel nozzle and connected to a streamlined forebody and cable support system.

The centerline pipe contained 55 static orifices (0.127-in. diam) spaced at 1-ft intervals from tunnel stations -5.9 to 0.1 and 0.5-ft intervals from tunnel stations 0.1 to 24.1. The pipe installation is shown in Fig. 2.

For test entries 1 and 2, wall static pressure distributions were obtained from two rows of pressure orifices installed in the floor 1 ft on either side of the test section centerline. A total of 24 orifices (0.065-in. diam) on the east side of the centerline were installed on a 2-ft-wide solid plate, which extended from tunnel stations 0 to 28. For test entry 2, the solid wall was extended upstream to tunnel station -9.0 by filling all holes in a single taper strip as shown in Fig. 2b. The solid wall orifices were installed on 1-ft centers from tunnel stations 0 to 20 and on 2-ft centers from tunnel stations 20 to 24. A total of 20 orifices (0.065-in. diam) on the west side of the centerline were installed in the perforated wall liners on 1-ft centers from tunnel stations 1 to 20.

During test entry 2, rows of orifices (0.65-in. diam) were installed in the perforated liners on the east and west walls and on the ceiling. A total of 9 orifices each were installed near the centerline of the east and west walls on 2-ft centers from tunnel stations 2 to 18. A total of 20 orifices were installed 1 ft west of the ceiling centerline on 1-ft centers from tunnel stations 1 to 20. For the orifices installed in the tunnel perforated wall liners, the four perforations adjacent to the orifices were filled with plaster as illustrated in Fig. 1.

The pipe orifices and wall pressure orifices were connected to differential pressure transducers which were referenced to the tunnel plenum chamber pressure. The tunnel stagnation pressure was determined by averaging measurements from two independent systems of total pressure probes installed in the tunnel stilling chamber. For calibration entry 1 the plenum chamber and stagnation pressures were determined by measurement from Ideal® self-balancing precision manometers. For calibration entry 2 the plenum chamber and stagnation pressures were determined by measurement from Datametrics® pressure sensors and electronic manometers.

3.0 PROCEDURE

3.1 TEST CONDITIONS

The calibrations were conducted over the Mach number range from 0.2 to 1.6; however, primary emphasis was placed upon Mach numbers above 0.55. Data were obtained at various stagnation pressures over a range from 400 to 4,000 psfa, which corresponds to unit Reynolds numbers from 0.5 to 6.0 x 10^6/ft. The effects of pressure ratio and wall angle variation were defined at a stagnation pressure of 1,600 psfa. This

stagnation pressure level was chosen as a baseline since the Ref. 2 and 3 calibrations were conducted primarily at 1,600 psfa. The tunnel stagnation temperature was maintained at 110°F for Mach numbers of 0.6 and above and at about 80°F for Mach numbers below 0.6.

On the basis of data presented in Ref. 3 and results obtained during this calibration, a nominal pressure ratio schedule was defined for utilization during variations of test section wall angle and Reynolds number. At subsonic Mach numbers the pressure ratio was selected as that associated with generally "flat" Mach number distributions. At supersonic Mach numbers a pressure ratio sufficient to keep the test section terminal shock wave system downstream of the model support strut was selected. The nominal pressure ratio (λ^*) schedule is shown in Fig. 3. To determine the effects of pressure ratio on the Mach number distributions, the pressure ratio was also varied during test entry 2 above and below the nominal schedule as shown in Fig. 3.

Test section wall angle was varied from 0.50 to -0.75 deg. Positive wall angles correspond to wall divergence from the tunnel centerline. The Tunnel 16T optimum wall angle schedule and the range of wall angles investigated during this calibration are shown in Fig. 4. The optimum wall angle schedule was defined in Ref. 5 as that which provided the "best" pressure distribution on long slender bodies of revolution with a test section blockage of one percent. The optimum wall angle schedule is used during AEDC NAB tests.

3.2 DATA REDUCTION

The distribution of local Mach number in the test section was obtained from the centerline pipe and wall static pressure data with the assumption of isentropic flow through the nozzle. The average Mach number and the 2σ Mach number deviation for three test section regions were computed. These include tunnel stations 1 to 20, which comprised the test region used for the Ref. 1 calibration, tunnel stations 3 to 19, which made up the test region used for the Ref. 6 calibration, and a test region from tunnel stations 6 to 18. The Mach number deviation, 2σ, is the conventional two standard deviation parameter utilized in statistical analysis.

The calibration of Tunnel 16T is based on the measured pressure differential between the test section and the plenum chamber at various operating conditions. An equivalent plenum chamber Mach number is calculated from plenum chamber and tunnel stagnation pressure measurements using the isentropic relationship. A calibration parameter, defined as the difference between the free-stream and plenum chamber Mach numbers ($M_\infty - M_c$), is utilized to express the tunnel calibration for various operating conditions.

3.3 DATA UNCERTAINTY

A Taylor series method of error propagation was utilized to estimate the uncertainty in the calibration parameters which could be attributed to instrumentation errors and data acquisition techniques. Uncertainties in the instrumentation systems were estimated from repeat calibration of the systems against secondary standards whose uncertainties are traceable to the National Bureau of Standards calibration equipment. For a confidence level of 95.4 percent, the estimated uncertainties are as follows:

Parameter	Uncertainty
λ	±0.002
θ	±0.04 deg
M	±0.002
M_∞	±0.0004
Re	±0.02 x 10^{-6}
$(M_\infty - M_c)$	±0.0019

The uncertainty in Mach number (M_∞) given above is that associated with the average of several local Mach numbers from the centerline pipe or wall orifices. For test operations the uncertainty in free-stream Mach number must also include provisions for the uniformity of the test section Mach number distributions and the repeatability of the tunnel calibration. These factors are illustrated in this report.

3.4 FLOW QUALITY

One of the primary objectives of a tunnel calibration is to ascertain that adequate flow quality exists for acquisition of test data for various locations of test models and various combinations of tunnel conditions. Tunnel flow quality encompasses several parameters, such as flow angularity and turbulence levels, which were not investigated during this calibration. Data presented in Ref. 6 indicate that undesirable axial Mach number gradients do not exist in Tunnel 16T for normal operating conditions. This report therefore will be concerned only with the uniformity of the axial Mach number distributions.

A quantitative evaluation of the uniformity of a Mach number distribution, when no pressure graidents exist, can be provided by analysis of the 2σ Mach number deviation. The minimum Mach number deviation for a particular test section length and set of tunnel conditions is, of course, indicative of the "best" distribution.

The author is unaware of any industry standard which exists for values of the 2σ Mach number deviations which are indicative of good Mach number distributions. For purposes of this report and in accordance with Ref. 2, 2σ Mach number deviations of $0.005M_\infty$ and $0.01\ M_\infty$ for subsonic and supersonic Mach numbers, respectively, will be utilized as criteria for the relative evaluation of the various Mach number distributions. These criteria should not be confused with tunnel data quality goals and requirements, which are established by facility test objectives.

4.0 RESULTS AND DISCUSSION

4.1 MACH NUMBER DISTRIBUTIONS

4.1.1 General

Tunnel 16T centerline and wall Mach number distributions were obtained at a variety of test conditions during the calibrations. The 2σ Mach number deviations for various test regions are utilized as an aid in evaluating the Mach number distributions. A complete and detailed presentation of all the calibration results is considered unnecessary. Accordingly, only selected data, sufficient to indicate various data variations as well as important results, are presented herein. Unless noted otherwise, the data presented were obtained during the second calibration entry.

Typical centerline and wall Mach number distributions obtained at Mach numbers from 0.2 to 1.6 with $\lambda = \lambda^*$, $\theta = 0$, and $P_t = 1,600$ psfa are presented in Figs. 5, 6, and 7. The data presented in Figs. 5 and 6 indicate that at subsonic Mach numbers. the rear portions of the centerline pipe and wall distributions differ. This is attributed to different interference effects at those locations. The distributions on the centerline are subject to interference effects from the support boom flare, the model support strut, and the test section wall bulge. The wall distributions, on the other hand, are subject to interference from the strut and wall bulge. For the case of the centerline distributions, it appears that the boom flare interference predominates. A detailed discussion of interference effects is beyond the scope of this report. It is sufficient to note that the data interferences observed for this test are generally consistent with those which can be found in the literature. The effects of the boom flare interference have no significant effect on the tunnel calibration (which will be discussed later) because the calibration is based on data upstream of tunnel station 20.

The data presented in Fig. 7 indicate that at supersonic Mach numbers the forward portions of the centerline pipe and wall distributions differ. According to Refs. 2 and 3, the supersonic centerline Mach number distributions were believed to be affected by

disturbances which emanated from the forward portion of the calibration pipe. Data presented in Figs. 7a and b tend to verify this possibility. The disturbances which occur (Fig. 7a) near tunnel stations -4, -2, and 0 for Mach numbers 1.4, 1.5, and 1.6, respectively, appear (by tracing Mach lines) to be caused by a reflection of the shock from the nose of the calibration pipe (tunnel station -22). The disturbance which exists at tunnel station 5 for $M_\infty = 1.2$ appears to emanate from near tunnel station 0. It is noted that the same disturbance also existed during the Ref. 2 and 3 calibrations. The fact that this disturbance seems to be unique to $M_\infty = 1.2$ warrants some study during a subsequent test.

The centerline pipe used for this calibration was fabricated for the Ref. 2 calibration. An effort was made to make this centerline pipe system satisfactory for acquisition of data at supersonic Mach numbers. The centerline pipe was considered adequate at supersonic Mach numbers for Refs. 2 and 3 because the calibration was based on the distributions downstream of tunnel station 8. The disturbances which are caused by the centerline pipe are of particular concern herein because the calibration for the aerodynamic test section has usually been based on the distributions in the forward portion of the test section.

4.1.2 Effects of Mach Number

Effects of Mach number on the 2σ Mach number deviations for the centerline distributions over two test regions are presented in Fig. 8 along with comparisons with previous calibrations. The data indicate that, except for $M_\infty \geqslant 1.2$, the deviations for the distributions over both test regions are better than the relative criteria for "good" distributions. The data also indicate that the centerline distributions compare reasonably well with the appropriate results from Refs. 3 and 6. The poor Mach number deviations at the high supersonic Mach numbers reflect the effects of the disturbances from the calibration pipe. Considering the sensitivity of the Mach number deviation parameter to small disturbances, the centerline distributions for Mach numbers of 1.2, 1.3, and 1.4 are considered to be of acceptable quality. It is also noted that the deviations over the test region from tunnel stations 3 to 19 are acceptable for $M_\infty = 1.5$, but not acceptable for $M_\infty = 1.6$.

4.1.3 Effects of Calibration Entry

The data presented in Fig. 9 provide comparison of the solid plate and porous wall Mach number deviations obtained during the two calibration entries. The data presented in Figs. 9a, 6b and c, and 7b and c indicate that Mach number distributions of comparable quality were obtained from the solid plate pressures during both calibration entries. The data presented in Fig. 9b indicate that the porous wall Mach number distributions for test entry 1 were of better quality than those for test entry 2. A

comparison of the solid plate Mach number deviations for the current and Ref. 1 calibrations is also shown in Fig. 9a. These data indicate that, except for $M_\infty \geqslant 1.4$, the deviations for the current calibration are slightly less than the deviations for Ref. 1. More importantly, however, both current calibration entries and Ref. 1 provided solid plate Mach number deviations equal to or better than the relative criteria for "good" Mach number distributions. As a consequence, presentation of Mach number distributions and deviations in the remainder of this report will be primarily restricted to data from the second calibration entry.

4.1.4 Effect of Pressure Orifice Selection

The data presented in Fig. 10 allow an evaluation of the various sets of wall pressure orifices. The pressure orifices in the solid plate clearly provide the smallest overall Mach number deviations and therefore the best Mach number distributions. For most Mach numbers, the pressure orifices in the porous wall provide Mach number deviations poorer than the relative criteria for "good" distributions. These poor quality data from the porous orifices are at least partly attributable to an orifice preparation effort consistent with the priority of the data. As a consequence of these results, presentation of wall data in the remainder of this report will be primarily restricted to that from the solid plates.

Comparisons of the Mach number deviations for the centerline distributions to those for the solid plate and porous wall Mach number distributions are presented in Fig. 11. The data in Fig. 11a indicate that the solid plate Mach number distributions are better than the centerline Mach number distributions. As was the case in Ref. 3, Fig. 11b indicates that the centerline Mach number distributions are much better than those derived from the porous wall pressures at subsonic Mach numbers. Since distributions of acceptable quality are available from both the centerline pipe and solid plate at most Mach numbers, either set of these data could be selected as the primary data set.

4.1.5 Effect of Test Region Length

The effect of test region on the Mach number deviations is presented in Fig. 12. These data indicate that at subsonic Mach numbers, only small differences exist between the deviations for the various test regions. For the centerline pipe data, the differences are partly attributable to the boom flare interference effects previously discussed (Fig. 6a). For the solid plate data, the differences are partly attributable to the effect of a small acceleration of the flow from tunnel station 0 to 2, which may be seen in Figs. 6b and c. This same trend in the distributions is shown in the data presented in Ref. 1. It is noted that this small disturbance is not as evident on the centerline (Fig. 6a) or the

porous plate (Figs. 6d and e). The observed disturbance with the solid plate is attributed to a step at station zero and the absence of the compensating characteristics of wall suction with the solid plate.

At supersonic Mach numbers the differences between the deviations which are shown in Fig. 12 for all three test regions are more pronounced than at subsonic Mach numbers for both the centerline and wall data. Considering the sensitivity of the 2σ parameter as an indicator of small disturbances, these differences are not considered significant except at $M_\infty = 1.2$, 1.5, and 1.6 for the centerline pipe data. It is noted that defining the test region as being from tunnel stations 6 to 18 provides significant improvement in the centerline Mach number deviations for these Mach numbers.

In view of the subsonic and supersonic Mach number results for various test regions, the test region from tunnel stations 6 to 18 is selected as the primary region for additional analysis of Mach number distributions. These results also indicate that this test region is the best region in which to position a model.

4.1.6 Effect of Tunnel Pressure Ratio

Centerline and wall (solid plate) Mach number distributions for various tunnel pressure ratios at Mach numbers from 0.8 to 1.2 for $\theta = 0$ and $P_t = 1,600$ psfa are presented in Figs. 13 and 14. These data indicate that the effects of pressure ratio variation are primarily restricted to the rear portion of the test section (usually downstream of tunnel station 20). Most test models are installed upstream of tunnel station 20.

The effects of pressure ratio variation on the 2σ Mach number deviations for tunnel stations 6 to 18 are presented in Fig. 15. The nominal pressure ratios (λ^*) are also illustrated. The data presented in Fig. 15 indicate that, except for the lower pressure ratios at $M_\infty = 0.8$, pressure ratio variation does not significantly affect the Mach number deviations for the selected test region. The lowest pressure ratio shown for each Mach number is not indicative of normal operating conditions in Tunnel 16T.

Data presented in Figs. 13 to 15 indicate that acceptable Mach number distributions can be obtained for various pressure ratios. The effect of pressure ratio variation on the auxiliary weight flow and tunnel power requirements is discussed in Appendix A.

The normal mode of operation in Tunnel 16T is to not vary tunnel pressure ratio or therefore utilize wall suction at $M_\infty < 0.75$. Data presented in Ref. 3 indicated that a tunnel total power savings might be achieved by using auxiliary weight flow at these

Mach numbers. The effects of varying tunnel pressure ratio on the centerline and wall Mach number distributions at $M_\infty \leqslant 0.75$ is illustrated in Fig. 16. The auxiliary weight flow ratio, ω, the 2σ Mach number deviation for tunnel stations 6 to 18, and the tunnel total power factor (mw/psf) are noted for each distribution. The data indicate that utilization of wall suction and a reduction of tunnel pressure ratio decelerates the flow at the downstream end of the test section. This effect, however, does not affect the 2σ Mach number deviations for tunnel stations 6 to 18. The data tabulated in Fig. 16 show that a total power savings from about 3 to 9 percent can be realized by reducing tunnel pressure ratio and using test section wall suction at $M_\infty \leqslant 0.75$. Since the quality of the Mach number distributions is not compromised and a power savings can be realized, these results warrant a change in tunnel operating procedures at $M_\infty < 0.75$.

4.1.7 Effect of Test Section Wall Angle

Centerline and wall Mach number distributions for various test section wall angles at Mach numbers from 0.2 to 1.6 with $\lambda = \lambda^*$ and $P_t = 1{,}600$ psfa are presented in Figs. 17 and 18. These data indicate that for subsonic Mach numbers, wall divergence decelerates the flow in the aft end of the test section. At supersonic Mach numbers, however, the effects of wall angle variation are not as definitive although they are restricted primarily to the forward portion of the test section. Typical effects of wall angle variation on the tunnel auxiliary flow and total power requirements are presented in Appendix A.

The effects of wall angle variation on the 2σ Mach number deviations for tunnel stations 6 to 18 are presented in Figs. 19 and 20. The test section wall angles associated with the optimum wall angle schedule, θ^*, (Fig. 4) are also noted. The data presented in Figs. 19 and 20 indicate that the effects of wall angle variation can be significant. At most Mach numbers, the best Mach number distributions were obtained either near zero or at slightly diverged wall angles. This result is consistent with that obtained in Ref. 3. Similar data were obtained when the wall angle was varied at other Reynolds numbers.

4.1.8 Effect of Reynolds Number

Centerline and wall Mach number distributions at various unit Reynolds numbers for Mach numbers from 0.2 to 1.6 with $\theta = 0$ and $\lambda = \lambda^*$ are presented in Figs. 21 and 22. These data indicate that variation of Reynolds number has only a small effect on the distributions. The effects of Reynolds number variation on the tunnel auxiliary flow and power requirements are discussed in Appendix A.

The effect of Reynolds number on the 2σ Mach number deviations for tunnel stations 6 to 18 is presented in Figs. 23 and 24. The effect of Reynolds number variations on the 2σ Mach number deviations at $M_\infty < 1.2$ is not considered significant. At $M_\infty \geqslant 1.2$, although the effects of Reynolds number variations on the Mach number can be significant, for most test conditions the resulting deviations are lower than the relative criteria for good distributions (see Fig. 8).

4.2 TUNNEL CALIBRATION

4.2.1 General

As indicated in Section 3.2, a Mach number parameter ($M_\infty - M_c$) is utilized to express the Tunnel 16T calibration. Analytic expressions of the Mach number calibration parameter are incorporated into facility computer programs for test operations. Test section Mach number is determined by using the calibration parameter and the equivalent plenum chamber Mach number which is calculated from tunnel plenum chamber and stagnation pressure measurements.

For the Ref. 1 calibration, linear equations with test section wall angle as a variable were utilized to express the calibration parameter. For the current calibration, as well as Refs. 2 and 3, analytic expressions of the Mach number calibration parameter were determined using a least-squares, multiple regression data fitting program. Several data fits were required to adequately specify the tunnel calibration at various test conditions.

The effect of the various calibration variables on the Tunnel 16T calibration is presented herein. Unless otherwise noted, the data presented were obtained during the second calibration entry.

The tunnel calibration parameter ($M_\infty - M_c$) is computed using the tunnel test section static, plenum chamber, and stagnation pressures. All three pressures and their measuring systems have different control and measurement response characteristics. The Tunnel 16T stagnation and plenum chamber pressures are independently and manually controlled. However, because the test section and plenum chamber communicate through the ventilated wall, the control of all three pressures and the Mach number are interrelated. As a consequence, the calibration parameter is very sensitive to transients in various tunnel parameters. Most of the scatter exhibited in the calibration data presented herein is attributed to such control transients. During acquisition of data at each test condition, data points were obtained until the tunnel calibration parameter had been repeated or the data scatter had been bracketed. At least three data points were

taken at each test condition. For many test conditions the repeatability of the calibration parameter is within ±0.0002. For nearly all conditions with P_t > 1,000 psfa, the repeatability of the calibration parameter is within ±0.001. For data at lower stagnation pressures, where pressure lag time becomes more significant, the repeatability of the calibration parameter increases to about ±0.002.

4.2.2 Effect of Mach Number

Effects of Mach number on the tunnel centerline Mach number distribution for two test regions are presented in Fig. 25. The data indicate that, except for M_∞ > 1.3, the calibration parameter increases with Mach number for θ = 0. The decrease in the calibration parameter at the high supersonic Mach numbers is attributed to the effects of the disturbances from the calibration pipe.

Comparison of the centerline calibration for a test region between tunnel stations 1 and 20 with the results from Ref. 3 is also presented in Fig. 25a. The data indicate that, except for M_∞ > 1.3, the two calibrations agree within about 0.001. Noting that the Ref. 3 calibration was conducted in test section 1 rather than test section 2, the data in Fig. 25a illustrate the typical difference in calibrations between the aerodynamic and propulsion test sections. Such a small difference is within the data uncertainty requirements for many test programs. For tests concerned with nozzle/afterbody drag, however, the small difference between the calibrations can become significant.

The centerline calibration for a test region between tunnel stations 3 and 19 is compared with the results from Ref. 6 in Fig. 25b. The Ref. 6 calibration was conducted using the aerodynamic test section. The data indicate excellent agreement between the two calibrations for M_∞ < 0.7. At the higher subsonic Mach numbers the disagreement is as large as 0.003. The Ref. 6 calibration was conducted using the Tunnel 4T calibration pipe. The supporting mechanism for that installation caused some interference at the high subsonic Mach numbers. A complete explanation for the large differences between the current calibration and Ref. 6 is not possible. Data presented in Ref. 7 indicate that the effect of the support interference would be to increase the downstream local Mach numbers and therefore the calibration parameter. This effect, however, does not account for all the difference between the calibrations. It does appear, however, that some of the difference can also be attributed to the data fairing used in Ref. 6.

4.2.3 Effect of Calibration Entry

The data presented in Fig. 26 provide a comparison of the solid and porous wall Mach number calibrations obtained during the two calibration entries. A comparison of

the solid wall results with the results from Ref. 1 is also shown in Fig. 26a. The data presented in Fig. 26b indicate that the calibrations based on the porous wall orifices agree within 0.0006. The data presented in Fig. 25a, however, do not reflect such good agreement between the three calibration entries. The solid plate calibrations for test entries 1 and 2 differ by as much as 0.002. The calibrated Mach number for test entry 1 is as much as 0.003 below that reported in Ref. 1. The calibrated Mach number for test entry 2, however, compares within ±0.0015 with the results from Ref. 1.

Although the differences in results between the various calibration entries cannot be specifically explained, a discussion of the possible reasons for the differences in the tunnel calibration is warranted. The differences could be simply attributable to the overall uncertainty and repeatability of tunnel calibration data. The bias shown in Fig. 26a between test entries 1 and 2, however, implies that the differences in the calibration parameter could be attributed to differences in the test setups and procedures.

The data for test entries 1 and 2 were obtained at precisely the same test conditions. The data for the Ref. 1 test were obtained at a stagnation pressure of 1,000 psfa and at slightly lower tunnel pressure ratios. Slightly higher tunnel pressure ratios were required for the current tests because of the installation of a new screen in the wind tunnel diffuser. Based on data presented in Ref. 3, however, the effects of the pressure ratio differences may be considered insignificant. The data presented in Ref. 3 also indicate that the effects of Reynolds number for most Mach numbers would cause the Ref. 1 data to be slightly higher (up to 0.0005) than that shown in Fig. 26a. Considering the effect of Reynolds number on the Ref. 1 data, the disagreement between Ref. 1 and the data from test entry 2 would either increase or decrease, depending upon the Mach number. However, the disagreement between the Ref. 1 calibration and the data from test entry 1 would be increased by considering the Reynolds number effect.

For all three test entries, the data reduction procedures were essentially the same. There were some differences, however, in the primary instrumentation, the number of instrument channels, and the instrumentation setup and calibration procedures. Test entry 1 and the Ref. 1 tests were conducted with the same primary instrumentation. For test entry 2, the instrumentation for measuring stagnation and plenum chamber pressure was different (see Section 2.2). The test section static pressures were measured with the same instrumentation for all three test entries. Since the calibration parameter ($M_\infty - M_c$) is calculated from several individual pressure measurements, care must be taken to ensure that the same instrument biases occur in each term of the calibration parameter. Such a precaution was taken for each current test entry. However, the possibility that some of the differences in tunnel calibration between the various test entries can be attributed to instrumentation differences cannot be discounted.

According to all available information, the same test installation was used for the Ref. 1 entry and test entry 1. The major difference between test entries 1 and 2 was the installation of the centerline pipe for test entry 2. The only other possible differences which could have existed would be changes of test section liner plates and whether or not the stabilizer region upstream of the test section solid plate was solid or porous. For Ref. 1 the stabilizer region was apparently all porous; however, the configuration could not be substantiated. For test entry 1 the stabilizer region was all porous. For test entry 2 a portion of the stabilizer region was solid as shown in Fig. 2b. During Tunnel 16T test installations, some of the test section perforated liner plates are frequently exchanged. Although the same test section was used for both current tests and the Ref. 1 test, there could have been a slight change in the overall pressure drop characteristics of the liner plate installations.

If the centerline pipe is accountable for the differences in the calibrations for test entries 1 and 2, which are shown in Fig. 26a, then it would be implied that the Tunnel 16T calibration is a function of model size. If this were the case, a test to evaluate the effect of model size would be warranted. It is not believed, however, that a model of such size (0.1-percent blockage) would affect the tunnel calibration. Moreover, if it had done so, then a better comparison between the results from test entry 1 and Ref. 1 should have been obtained.

In summary, the differences between the calibrations for both current test entries and the Ref. 1 test can be attributed to changes in primary instrumentation, the test section liner plate characteristics, and the repeatability of the calibration data. Considering the nature of these factors, it is impossible to determine, without some reservations, which test provided the "best" calibration data. Because 1) they are the most recently available data, 2) the centerline pipe was installed, and 3) new primary instrumentation was used, the data from test entry 2 will be used to define the Tunnel 16T calibration.

4.2.4 Effect of Pressure Orifice Selection

The selection of a primary set of data from the various available pressure distributions is required to define the tunnel calibration. Comparisons of the tunnel calibration based on the centerline pipe, solid wall, and porous wall Mach number distributions are presented in Fig. 27.

The data presented in Fig. 27a indicate that except for M_∞ = 1.6 the calibrations based on the centerline pipe and solid wall Mach number distributions from tunnel stations 3 to 19 agree within 0.0008. The calibration parameter for the solid wall is also consistently above that for the centerline pipe. Although the porous wall data agree fairly well with the centerline pipe and solid wall data at many Mach numbers, unsatisfactory agreement is obtained at several Mach numbers.

The data presented in Fig. 27b indicate that at subsonic Mach numbers the porous bottom wall orifices provide the same calibration as the centerline pipe. At supersonic Mach numbers (except M_∞ = 1.6) the porous bottom wall and centerline pipe calibration agree within ±0.002. The data in Fig. 27b also indicate that the top and bottom porous wall calibrations disagree significantly (up to 0.007). This poor agreement is attributed largely to poor quality of the pressure orifices on the top wall (see Fig. 10).

The porous bottom wall results presented in Fig. 27 imply that porous wall pressure orifices could be utilized to define the tunnel calibration for θ = 0. However, the porous wall orifices must be properly located and prepared (see Fig. 1a) if accurate calibration data are desired. Data presented in Ref. 1 indicate that at supersonic Mach numbers and converged test section wall angles the porous plate orifices can provide significantly erroneous calibration data. Data obtained during this test, but not presented herein, confirm these Ref. 1 results. As a consequence, it is concluded that porous wall orifices should not be utilized for a general tunnel calibration.

The data presented in Fig. 27c indicate that the calibrations from the centerline pipe and solid wall orifices are in good agreement at subsonic Mach numbers. For supersonic Mach numbers the solid wall and centerline calibrations using tunnel stations 6 to 18 agree within ±0.0015. Except for M_∞ = 1.6, the solid wall data at supersonic Mach numbers are higher than the centerline pipe data. It is not considered possible to provide an adequate and unquestionable explanation for the small differences between the calibrations from these two sets of orifices. The small differences in calibration, the need to provide the best possible calibration, and the uncertainty of the calibration data make it very difficult to make a choice between the centerline pipe and solid wall data for defining the tunnel calibration. Slightly lower 2σ Mach number deviations (Figs. 11 and 12) and the fact that the cost of conducting calibrations with the solid plate installed are significantly less than with the centerline pipe favor the use of the solid wall orifices. The fact that test models are installed near the tunnel centerline rather than the wall constitutes a basis for selection of the centerline pipe. According to Ref. 8, the centerline pipe is the preferred, although not the universal method, of measuring the test section static pressure for transonic wind tunnel calibration. The centerline pipe is selected to define the calibration in this report.

4.2.5 Effect of Test Region Length

The effect of test region on the centerline Mach number calibration is presented in Fig. 28. These data indicate that at subsonic Mach numbers varying the test region as shown does not have a significant effect on the tunnel calibration. At supersonic Mach numbers, except for $M_\infty = 1.5$ and 1.6, the calibrations based on the various test regions agree within ±0.0005. At $M_\infty = 1.5$ and 1.6, the calibration based on tunnel stations 6 to 18 is significantly different from those for the other two test regions. This difference is attributed to the removal of the effects of the disturbances from the nose of the calibration pipe. Based on these and other results presented herein, the test region from tunnel stations 6 to 18 is selected for defining the Tunnel 16T calibration in this report.

4.2.6 Effect of Tunnel Pressure Ratio

The effects of tunnel pressure ratio variation on the Tunnel 16T calibration with $\theta = 0$ and $P_t = 1,600$ psfa are presented in Fig. 29. The data indicate that for the normal tunnel operating range ($\lambda > 1.16$) pressure ratio variation has no significant effect on the tunnel calibration for $M_\infty \geq 0.8$. As a consequence, the calibration is defined independent of the tunnel pressure ratio for this Mach number range.

The data presented in Fig. 29b indicate that utilization of wall suction at $M_\infty \leq 0.75$ reduces the Mach number calibration parameter by as much as 0.001 at $M_\infty = 0.6$. In view of the change in calibration parameter relative to the change in pressure ratio, the effects of pressure ratio variation can be significant at $M_\infty \leq 0.75$. However, considering the Mach number distributions (Fig. 16), the lowest pressure ratios shown in Fig. 29b for each Mach number should be the minimum ever used. Restricting the pressure ratios to such values minimizes the effect of varying pressure ratio on the tunnel calibration at $M_\infty \leq 0.75$.

4.2.7 Effect of Test Section Wall Angle

The Tunnel 16T aerodynamic test section calibration at $\theta = 0$ and $P_t = 1,600$ psfa for Mach numbers from 0.2 to 1.6 is presented in Fig. 30. The calibration data are based on the Mach number distributions from tunnel stations 6 to 18. The curve shown results from calculations using a least-square polynomial curve fit of the respective data. The coefficients associated with the curve fit are presented in Table 1. The maximum residual (the difference between the actual and computed values) which results from the curve fit is 0.0017. However, 95 percent of the data have residuals within 0.0008. The residuals and coefficients which result for fitting the data for two Mach number ranges are also presented in Table 1. Since the higher residuals occur at supersonic Mach number, particularly $M_\infty = 1.3$ and 1.5, the improvement obtained with this procedure is not significant.

23

The data presented in Fig. 30 at Mach numbers from 0.6 to 0.75 include those obtained both with and without wall suction. The data indicate that the effects of using wall suction at the low subsonic Mach numbers is distinguishable. The effect of adding wall suction causes the rather large changes in slope near $M_\infty = 0.75$ which are evident in most of the calibration curves presented in Figs. 25 to 28. Although no data were obtained with wall suction below $M_\infty = 0.6$, the data in Fig. 30 indicate that the calibration at lower Mach numbers would also be affected. Utilization of wall suction at Mach numbers from 0.6 to 0.75 is recommended because of the available tunnel power savings. However, because of the repeatability of the calibration data and because the procedure provided the best overall data fit, the data both with and without wall suction were utilized to define the tunnel calibration at $\theta = 0$ and $P_t = 1,600$ psfa.

A comparison of the current aerodynamic test section results with the Ref. 2 propulsion test section results is also presented in Fig. 30. The analytic results from Ref. 2 are currently utilized during Tunnel 16T operations. The data show that except for $M_\infty \geqslant 1.5$ the two curve fits agree within ±0.0015. Because of the need for improving data quality, it is recommended that the current data be utilized for the tunnel calibration with the aerodynamic test section at $\theta = 0$ and $P_t = 1,600$ psfa.

The effects of test section wall angle variation on the Tunnel 16T calibration with $\lambda = \lambda^*$ and $P_t = 1,600$ psfa are illustrated in Fig. 31. These data indicate that the calibration is significantly affected by wall angle variation. Calibration data fits are therefore required as a function of wall angle. The solid curves shown in Fig. 31 depict the analytic surface which corresponds to the results of the data-fitting program. The coefficients associated with the current data surface fit for various wall angles are presented in Table 2. This surface fit results in maximum residuals of 0.0011 for 95 percent of the data. Some improvement in the residuals can be achieved at subsonic Mach numbers by fitting the data in two ranges (see Table 2).

A comparison with the Ref. 2 results is also presented in Fig. 31. Results from the current test agree with the Ref. 2 surface fits within ±0.002 for most test conditions. Wall angles other than zero and those associated with the optimum wall angle schedule are rarely used in Tunnel 16T. At optimum wall angles (θ^*), for $1.1 \leqslant M_\infty \leqslant 1.4$ the agreement between this test and Ref. 2 is within 0.001. A comparison (omitted from Fig. 31 for clarity) of the current results with the aerodynamic test section results from Ref. 1 indicated data agreements similar to the agreement obtained with Ref. 2. To be consistent with the approach adopted for $\theta = 0$, it is also recommended that the current calibration data be utilized at $\theta \neq 0$ with the aerodynamic test section. Results presented in Ref. 3 should be utilized for the tunnel calibration with the propulsion test section for both $\theta = 0$ and $\theta \neq 0$.

4.2.8 Effect of Reynolds Number

Early calibration experience in Tunnel 16T indicated that Reynolds number did not have a significant effect on the tunnel calibration. As a consequence stagnation pressure has usually not been selected as a variable during tunnel calibration. The Ref. 1 calibration was conducted at 1,000 psfa. The Ref. 6 calibration was conducted at a constant Reynolds number of 3.0 x 10^6/ft, which corresponded to a stagnation pressure variation of about 1,500 to 2,000 psf. The data presented in Ref. 6 indicated that the calibrated Mach number was consistently above but within 0.001 of that for Ref. 1 at most test conditions, and such differences were considered negligible. As indicated in Ref. 3, however, the effect of Reynolds number for some tests in Tunnel 16T with the propulsion test section can be significant. The effects of Reynolds number on the Tunnel 16T aerodynamic test section wall and centerline Mach number calibration at various test section wall angles are illustrated in Figs. 32 to 37.

A comparison of some of the current Reynolds number calibration results with selected results from Ref. 3 is presented in Fig. 32. The Ref. 3 data presented in Fig. 32 indicate that at low Reynolds numbers a minimum and change in curve slope were consistently obtained. Based on the results from Ref. 2, such a trend was not expected. The reason for this data trend was not completely explained in Ref. 3 although pressure system lag time was recognized as a potential problem at the lower Reynolds numbers. The current centerline calibration data in Fig. 32 indicate that the same data trend partially exists at low Reynolds numbers since there is a trend of decreasing curve slope with decreasing Reynolds number. It is noted that the wall calibration data, which will be shown in Fig. 34, show no sign of this effect. In fact, a slightly increasing slope with decreasing Reynolds number is depicted by the data. These results pose the question of whether differences may be caused by measuring the static pressure on the centerline pipe or the test section wall.

The data presented in Fig. 32 also indicate that except for low Reynolds numbers, the tunnel calibrated Mach number increases slightly with increasing Reynolds number. Such a small effect could justifiably be neglected for most types of tunnel test programs. For nozzle afterbody tests, however, such effects can be significant. Because the trends with Reynolds numbers are consistent and repeatable, a correction to the tunnel calibration for Reynolds number effects can be made. It is also noted that the effect of increasing Reynolds number is more significant for the current aerodynamic test section calibration than for Ref. 3 with the propulsion test section. This difference as well as the difference in the magnitude of the calibration parameter justifies separate calibrations for the aerodynamic and propulsion test sections.

The typical effects of utilizing Ref. 1 and neglecting the Reynolds number effects on model test data are illustrated in Fig. 33. The average pressure coefficient is the average of local coefficients over the test region from tunnel stations 6 to 18 and is based on the free-stream static and dynamic pressures resulting from the Ref. 1 calibration. Clearly, the average pressure coefficient for a test region will be zero if the tunnel free-stream static pressure determined from the tunnel-calibrated Mach number is equal to the average of the measured static pressure over the test region of interest. The data presented in Fig. 33 indicate that except for $M_\infty = 0.6$ the error in pressure coefficient caused by neglecting Reynolds number effects is less than ±0.005.

The calibrations based on test section solid plate pressures for both current calibration entries and the optimum test section wall angle schedule are presented in Fig. 34. The data indicate that fairly consistent and significant differences exist between the calibration entries. The possible reasons for these differences were discussed in Section 4.2.3. The data in Fig. 34 do indicate, however, that effect of Reynolds number on the calibration is similar for the two test entries.

As previously indicated, the centerline pipe data rather than the wall data will be utilized to define the tunnel calibration. The calibration based on solid plate pressure results from test entry 1, however, were utilized to correct data from some test programs for the effects of Reynolds number. For the correction program second-order curve fits of the data were utilized. To document these results, the coefficients for the curve fits for specific Mach numbers with $\theta = \theta^*$ are presented in Table 3. The calibrated parameter was expressed as a function of stagnation pressure, rather than Reynolds number, because pressure is an independent variable.

The effect of Reynolds number on the centerline Mach number calibration for $\theta = 0$ is presented in Fig. 35. The calibration data shown are based on the Mach number distributions from tunnel stations 6 to 18. Considering the data fits necessary to account for various calibration parameters and available online computer storage, the data presented in Fig. 35 were fit, as was done in Ref. 3, to a family of linear curves which pass through the data at $P_t = 1,600$ psfa. The data fairings are extrapolated to the approximate maximum available Reynolds number for each Mach number.

The data presented in Fig. 35 indicate that for most test conditions the Mach number varies by less than ±0.003 for variation of Reynolds number over the available range. The largest Reynolds number effect is obtained at $M_\infty = 0.6$, which agrees with the results from Ref. 3. For Mach numbers from 0.6 to 1.5, the effects of Reynolds number on the tunnel calibration tend to decrease with increasing Mach number. The same trend was obtained for Ref. 3 for Mach numbers from 0.6 to 1.6. The fact that the current $M_\infty = 1.6$ data do not follow this trend causes these data to be somewhat suspect.

26

Utilization of the linear fairing in Fig. 35 yields uncertainties in Mach number of up to 0.002 at P_t < 1,000 psfa, but usually less than 0.0005 at P_t ≥ 1,000 psfa. Data at low pressures are rarely obtained in Tunnel 16T. As a consequence, the Mach number errors resulting from this simplification of the data reduction program are considered acceptable.

The data at M_∞ = 0.6 shown in Fig. 35 were obtained without wall suction. It is suspected that the larger effects of Reynolds number at M_∞ = 0.6 could be attributed to this fact. As a consequence it is possible that utilization of suction at M_∞ ≤ 0.75 could reduce the effects of Reynolds number. This possibility should be investigated during a subsequent calibration.

Limited data were obtained to define the overall effects of wall angle variation on the Reynolds number calibration. These results are presented in Fig. 36. The data indicate that the Reynolds number effects can change with variation in wall angle. The relative magnitudes of the changes and the capability to account for them, however, is of particular significance. At subsonic Mach number, for example, when linear curves of the same slope as that at θ = 0 are fit through the data in Fig. 36 for θ ≠ 0, a fair data fit is obtained. Since the worst discrepancy is small and occurs at the lowest Reynolds numbers and the wall angle is rarely varied from θ = 0 at M_∞ < 1.0 in Tunnel 16T, the resulting data fits are considered satisfactory. As a consequence, the effects of wall angle on the Reynolds number calibration may be neglected at subsonic Mach numbers. The effects of wall angle variation on the tunnel calibration are accounted for by the surface fit shown in Fig. 31.

The data presented in Fig. 36 also indicate that the effects of wall angle variation on the slopes of the data fairings are more significant at supersonic than at subsonic Mach numbers. However, large changes in the slopes of the data fairings can be made which produce small (±0.001) variations in Mach number. For most test programs, therefore, the effect of wall angle variation on the Reynolds number calibration at supersonic Mach numbers may be neglected.

To obtain the maximum accuracy and for complete generality, the tunnel calibration for Tunnel 16T must be expressed for all potential Mach numbers, wall angles, and Reynolds numbers. Considering the results presented herein and in Ref. 3, such a data set cannot be satisfactorily fit with a hypersurface. Consequently, more than one set of data fits and coefficients are utilized to express the tunnel calibration. Following the approach in Ref. 3, a primary calibration pressure of 1,600 psfa was selected so that analytical expressions and coefficients presented in Tables 1 and 2 might be utilized to compute the

tunnel Mach number at all wall angles for P_t = 1,600 psfa. The correction for Reynolds number is then obtained by accounting for the differences in the calibration from P_t = 1,600 psfa.

Changes in the calibration parameter (M_∞ - M_c) as a linear function of stagnation pressure were used to obtain a family of curve slopes for use in the correction routine. Variation of the slopes, $\Delta(M_\infty$ - $M_c)$/psf, for θ = 0 and θ = θ^* as a function of Mach number is presented in Fig. 37. So that the Reynolds number correction routine may be used for any tunnel test condition, the slopes of the linear curves were fit by various polynominals. The coefficients for various slope data fits and the equations for correcting Mach number for Reynolds number effects are presented in Tables 4 and 5.

The fairings shown in Fig. 37 result from computations using the data fits. The best results were obtained when the range of data to be fitted was selected by Mach number and/or test section wall angle schedule. Before an acceptable fit of the data could be obtained at most Mach numbers some soothing of the supersonic Mach number data was necessary. The deviations of the smoothed data from the overall data trend are attributed partly to the fact that adequate data were not available to establish a slope. However, the effect of this data smoothing on the tunnel calibration is small. For example, for a slope change of ±1.0 x 10^6/psf the effect on Mach number is ±0.001/1,000 psf. At supersonic Mach numbers a ±1,000-psf variation in stagnation pressure from 1,600 psf completely encompasses the normal tunnel operating range.

The data presented in Tables 4 and 5 allow several choices to correct for the effects of Reynolds number in Tunnel 16T. The simplest approach, which is considered satisfactory for most test programs, is to neglect the effect of wall angle (Table 4) for the entire Mach number range of Tunnel 16T. The differences between the slope data in Fig. 37 for θ = 0 and θ = θ^* provide an indication of the result of neglecting the effects of wall angle at supersonic Mach numbers. To diminish the effect of the approach, data fits based on the average of the θ = 0 and θ = θ^* data may be utilized in correcting for the effects of Reynolds number (Table 5). Finally, these corrections may be made for tests which specifically utilize the optimum wall angle schedule (θ^*) (Table 4 for M $\leqslant$ 1.0 and Table 5 for M $\geqslant$ 1.05).
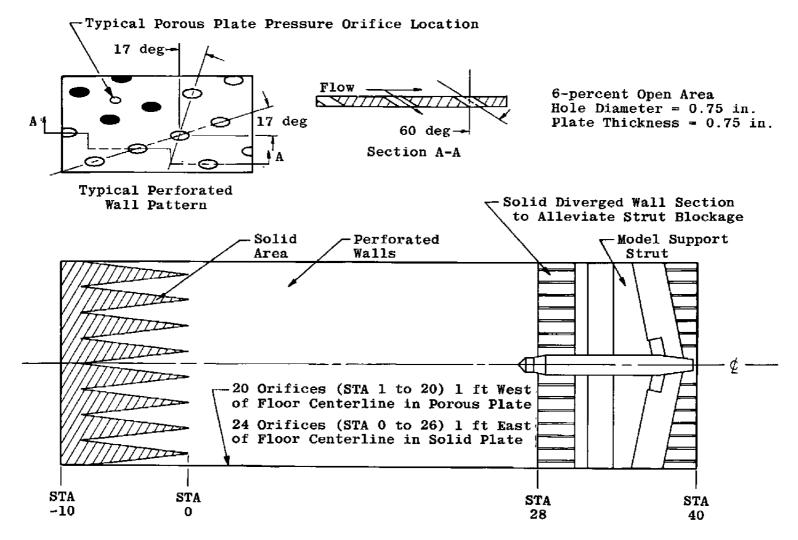
5.0 CONCLUSIONS

Based on the results from this test to define the effects of Reynolds number variation on the Tunnel 16T aerodynamic test section Mach number distributions and calibration, the following conclusions have been reached:

1. Variation of tunnel pressure ratio over a normal operating range has no significant effect on either the Mach number distributions and or the calibration.

2. Variation of test section wall angle can have a significant effect on both the Mach number distributions and the calibration.

3. Variation of Reynolds number has a negligible effect on the Mach number distributions for Mach numbers less than 1.2.

4. Variation of Reynolds number has a small but definable effect on the Tunnel 16T Mach number calibration.

5. Although for most test conditions the current tunnel calibration agrees with previous results (within ±0.0015), some changes in the tunnel calibration are desirable.

6. The Tunnel 16T Mach number calibrations based on centerline and solid plate pressure distributions agree within ±0.0015.

7. For maximum accuracy, the Tunnel 16T calibration must be defined as a function of test section wall angle, Reynolds number, and Mach number. Analytical expressions which adequately represent the tunnel calibration at various test conditions were developed.

8. Variation of tunnel pressure ratio can have a significant effect on tunnel total power requirements. Generally, the minimum power requirements correspond to the minimum pressure ratios which provide "flat" Mach number distributions to tunnel station 20.

9. Variation of test section wall angle can have a significant effect on the tunnel total power requirements. Generally, the minimum power requirements were obtained at zero or slightly diverged wall angles.

10. Utilization of wall suction at Mach numbers from 0.6 to 0.75 provides a tunnel total power savings from about 3 to 9 percent.
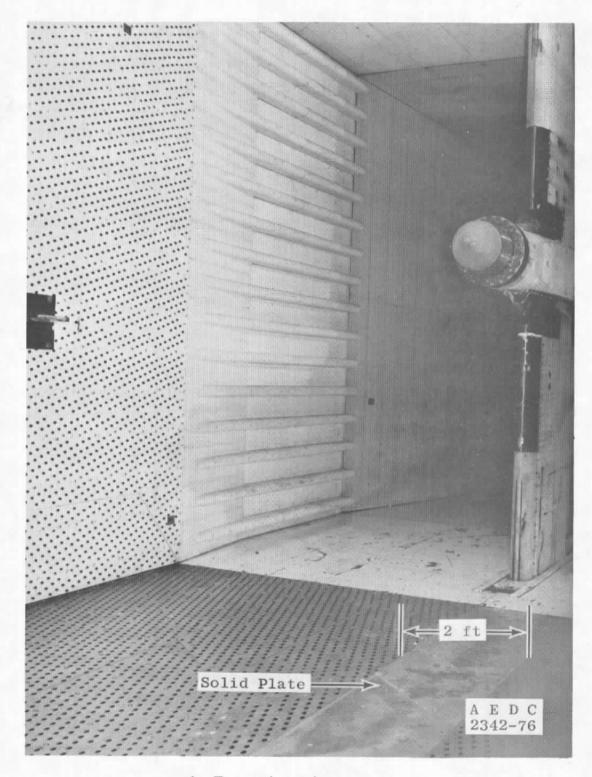
REFERENCES

1. Gunn, J. A. "Check Calibration of the AEDC 16-Ft Transonic Tunnel." AEDC-TR-66-80 (AD633277), May 1966.

2. Jackson, F. M. "Calibration of the AEDC-PWT 16-Ft Transonic Tunnel at Test Section Wall Porosities of Two, Four and Six Percent." AEDC-TR-76-13 (ADB008985L), January 1976.

3. Jackson, F. M. "Calibration of the AEDC-PWT 16-Ft Transonic Tunnel with the Propulsion Test Section at Various Reynolds Numbers." AEDC-TR-77-121 (ADA057877), February 1977.

4. Test Facilities Handbook (Tenth Edition). "Propulsion Wind Tunnel Facility, Vol. 4." Arnold Engineering Development Center, Arnold Air Force Station, Tennessee, May 1974.

5. Nichols, James H. "Determination of Optimum Operating Parameters for the PWT 16-Ft Transonic Circuit Utilizing One-percent Bodies of Revolution." AEDC-TN-59-100 (AD225362), September 1959.

6. Jackson, F. M. "Supplemental Calibration Results for the AEDC Propulsion Wind Tunnel (16T)." AEDC-TR-70-163 (AD872475), August 1970.

7. Dick, R. S. "The Influence of Several Cable-Type Supports upon the Static Pressures Along the Centerline Tube in a Transonic Wind Tunnel." AEDC-TN-54-26, January 1955.

8. Reed, T. D., Pope, T. C., and Cooksey, J. M. "Calibration of Transonic and Supersonic Wind Tunnels." NASA CR 2920, November 1977.

Typical Porous Plate Pressure Orifice Location

17 deg

A

17 deg

A

Typical Perforated
Wall Pattern

Flow

60 deg

Section A-A

6-percent Open Area
Hole Diameter = 0.75 in.
Plate Thickness = 0.75 in.

Solid Diverged Wall Section
to Alleviate Strut Blockage

Solid
Area

Perforated
Walls

Model Support
Strut

20 Orifices (STA 1 to 20) 1 ft West
of Floor Centerline in Porous Plate

24 Orifices (STA 0 to 26) 1 ft East
of Floor Centerline in Solid Plate

¢

STA
-10

STA
0

STA
28

STA
40

31

a. Test installation

Figure 1. Tunnel 16T calibration installation (test entry 1).

Solid Plate

2 ft

A E D C
2342-76
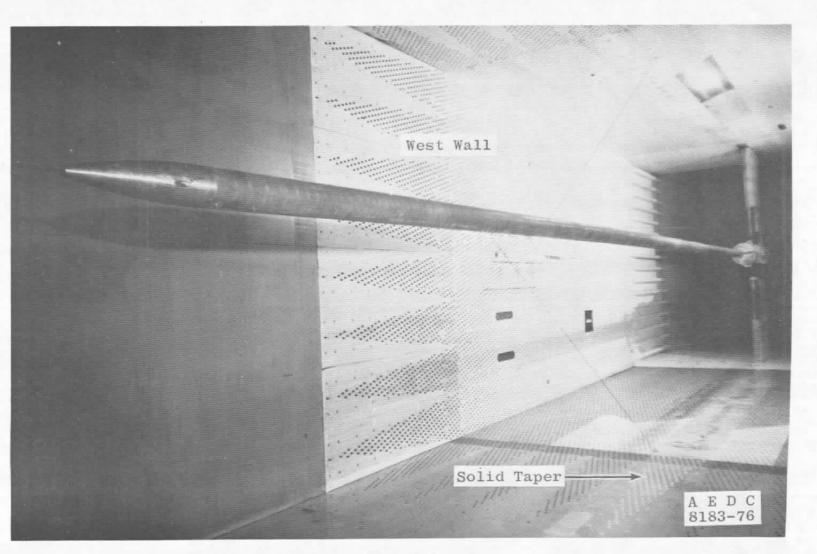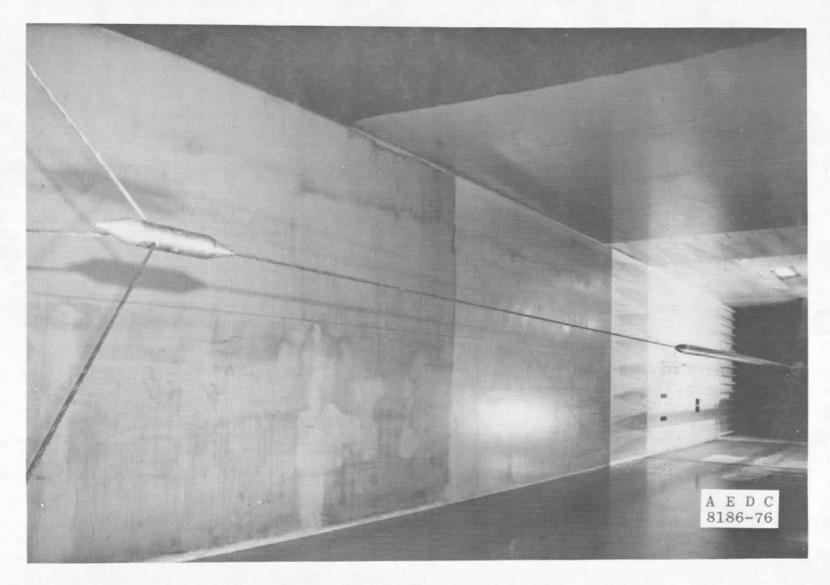
b. Test section and support strut
Figure 1. Concluded.

Typical Porous Plate
Pressure Orifice Location

17 deg

17 deg

Notes: (1) 44 Floor Orifices, Same as Test
            Entry 1 (See Fig. 1a)
        (2) 20 Ceiling Orifices (STA 1 to 20)
            1 ft West of Centerline in Porous Plate
        (3) 9 Orifices (STA 2 to 18) Near Centerlines
            of Both East and West Walls in Porous Plate

Typical Perforated
Wall Pattern

Solid Diverged Wall Section
to Alleviate Strut Blockage

Solid   Perforated   Model Support
Area   Walls   Strut

30 deg

Cable   Cable

0.5-ft diam Centerline Pipe

Cable

48 Orifices, 0.5-ft Spacing

7 Orifices, 1-ft Spacing

STA   STA   STA   STA   STA   STA   STA   STA
-22   -12.3   -10   0   5   24   28   40

Stations in Feet

a. Test installation

Figure 2. Tunnel 16T calibration installation (test entry 2).

33

West Wall

Solid Taper

A E D C
8183-76

b. Pipe and main supporting cables
Figure 2. Continued.

c. Pipe and forward cable system
Figure 2. Continued.

AEDC-TR-78-60

d. Pipe and rear mount system
Figure 2. Concluded.

Note: For $\lambda \neq \lambda*$ and $M_\infty \geq 0.8$, $\theta = 0$

Nominal Pressure
Ratio Schedule ($\lambda*$)

Test Envelope
with Auxiliary
Suction (Test
Entry 2 Only)

No Auxiliary Suction, $\theta = 0$

Tunnel Pressure Ratio (λ)

1.50
1.40
1.30
1.20
1.10
1.00

0.1   0.3   0.5   0.7   0.9   1.1   1.3   1.5   1.7

Mach Number (M_∞)
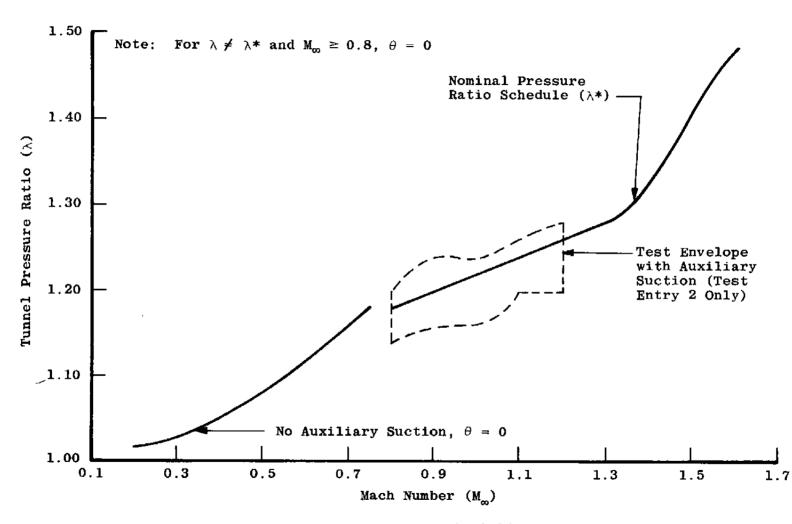
Figure 3. Tunnel pressure ratio schedules.

Test Section Wall Angle (θ), deg

0.8

0.4

0

-0.4

-0.8

-1.2

Optimum Wall Angle
Schedule ($\theta*$)

Test Envelope

0.1 0.3 0.5 0.7 0.9 1.1 1.3 1.5 1.7

Mach Number (M_∞)
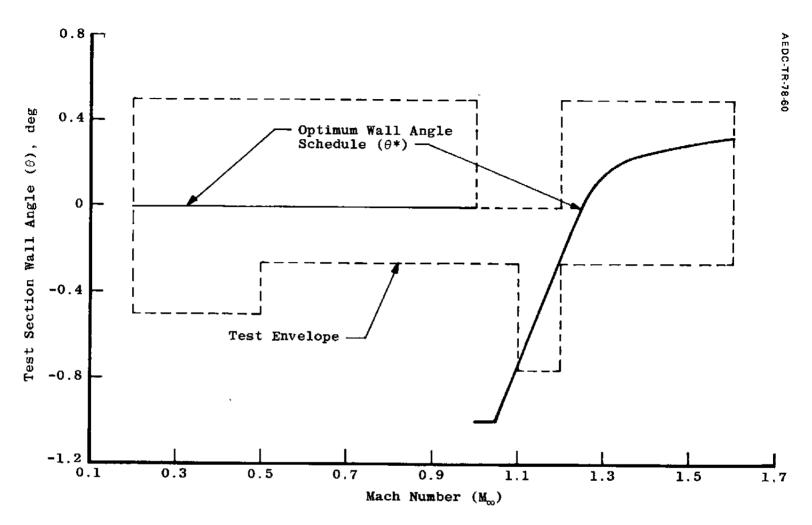
Figure 4. Test section wall angle schedules.
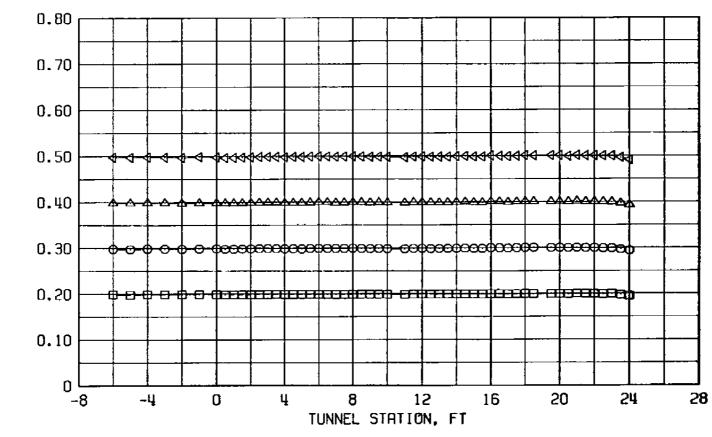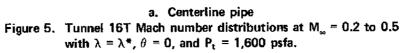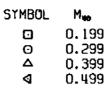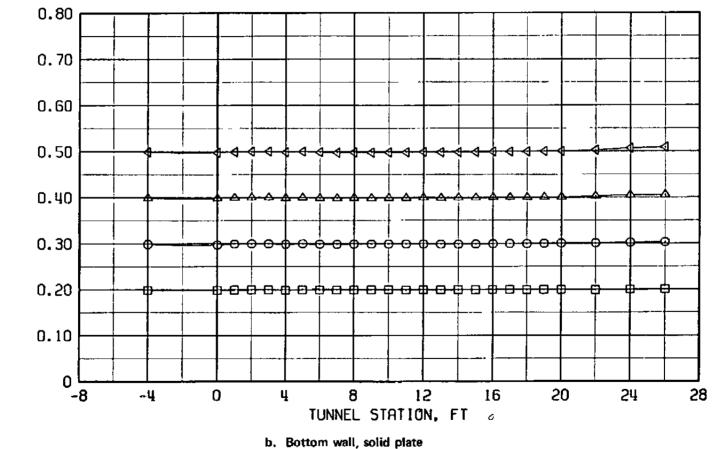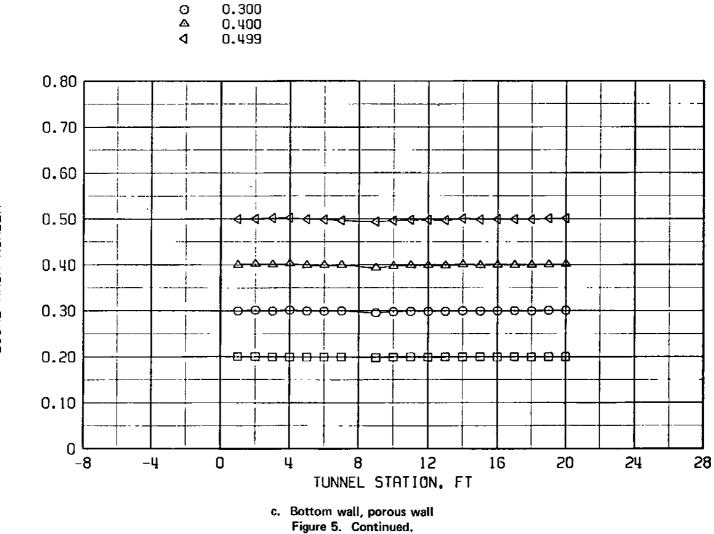
a. Centerline pipe

Figure 5. Tunnel 16T Mach number distributions at M_∞ = 0.2 to 0.5 with $\lambda = \lambda^*$, $\theta = 0$, and P_t = 1,600 psfa.

b. Bottom wall, solid plate
Figure 5. Continued.

SYMBOL M_{∞}
⊡   0.200
⊙   0.300
△   0.400
◁   0.499

c. Bottom wall, porous wall
Figure 5. Continued.
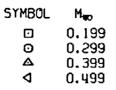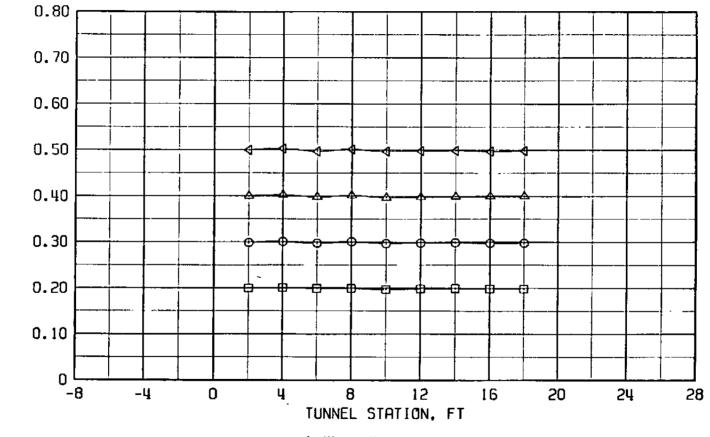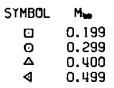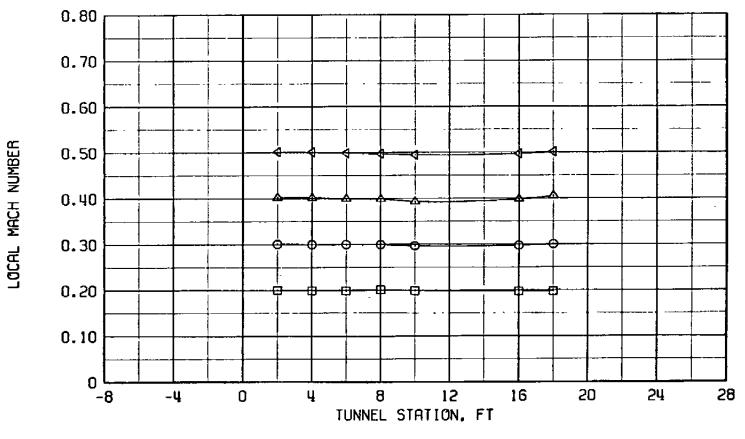
d. West wall
Figure 5. Continued.

e. East wall
Figure 5. Continued.

SYMBOL	M_∞
⊡	0.200
⊙	0.300
△	0.401
◁	0.500
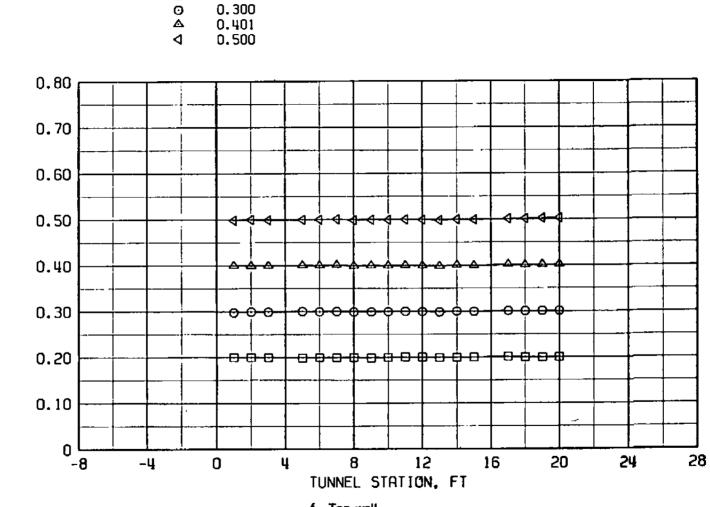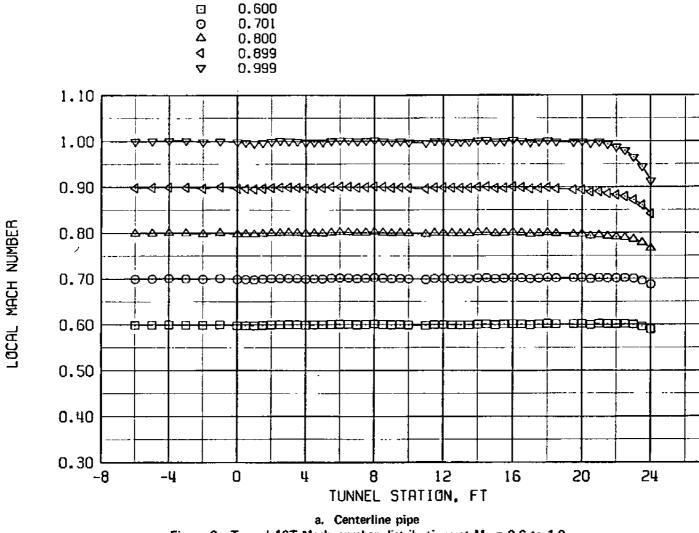
f. Top wall
Figure 5. Concluded.

a. Centerline pipe

Figure 6. Tunnel 16T Mach number distributions at M_∞ = 0.6 to 1.0 with $\lambda = \lambda^*$, $\theta = 0$, and P_t = 1,600 psfa.

b. Bottom wall, solid plate (test entry 2)
Figure 6. Continued.

c. Bottom wall, solid plate (test entry 1)
Figure 6. Continued.

d. Bottom wall, porous wall (test entry 2)

Figure 6. Continued.

SYMBOL M_∞
☐   0.600
⊙   0.701
△   0.801
◁   0.901
▽   1.002

LOCAL MACH NUMBER

TUNNEL STATION, FT

e. Bottom wall, porous wall (test entry 1)
Figure 6. Continued.

f. West wall
Figure 6. Continued.

SYMBOL M_∞

▫	0.602
⊙	0.703
△	0.804
◁	0.903
▽	1.004

g. Top wall
Figure 6. Continued.

SYMBOL M_∞

⊡	0.601
⊙	0.702
△	0.802
◁	0.901
▽	1.002
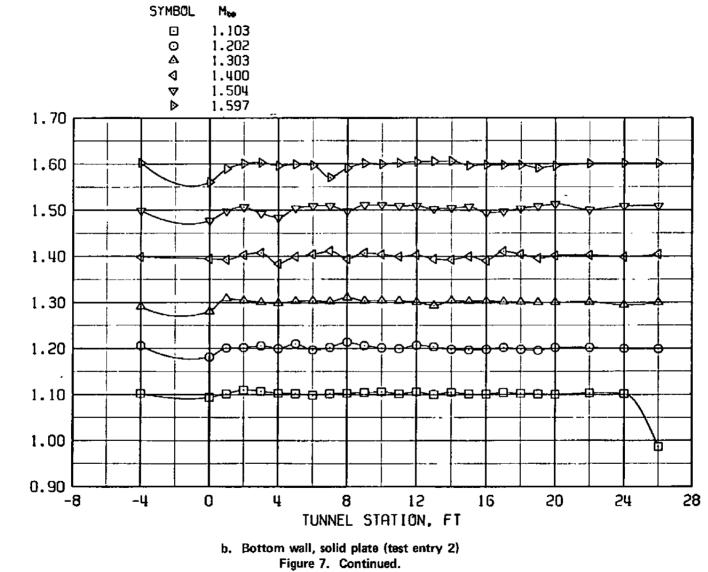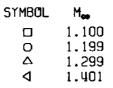
h. East wall
Figure 6. Concluded.

a. Centerline pipe

Figure 7. Tunnel 16T Mach number distributions at M_∞ = 1.1 to 1.6 with $\lambda = \lambda^*$, $\theta = 0$, and P_t = 1,600 psfa.

b. Bottom wall, solid plate (test entry 2)
Figure 7. Continued.

SYMBOL   M∞
□   1.100
○   1.199
△   1.299
◁   1.401

c. Bottom wall, solid plate (test entry 1)
Figure 7. Continued.

SYMBOL   M∞

□	1.101
⊙	1.199
△	1.300
◁	1.399
▽	1.501
▷	1.599

d. Bottom wall, porous wall (test entry 2)
Figure 7. Continued.

SYMBOL M_∞
□   1.100
○   1.199
△   1.299
◁   1.401

e. Bottom wall, porous wall (test entry 1)
Figure 7. Continued.

f. West wall
Figure 7. Continued.

g. Top wall
Figure 7. Continued.

h. East wall

Figure 7. Concluded.

a. Tunnel stations 1 to 20
Figure 8. Effect of Mach number on the centerline Mach number
deviations with $\lambda = \lambda^*$, $\theta = 0$, and P_t = 1,600 psfa.

b. Tunnel stations 3 to 19
Figure 8. Concluded.

0.032

0.028

○   Entry 2

□   Entry 1

━ ━   Ref. 1 (Test Section 2, P_t = 1,000 psfa)

0.024

Note: 2σ Deviations for Tunnel
        Stations 1 to 20

0.020

0.016

Relative Criteria
for "Good" Mach
Number Distributions

0.012

0.008

0.004

0

0   0.2   0.4   0.6   0.8   1.0   1.2   1.4   1.6   1.8

Mach Number (M_∞)

2 Mach Number Deviation

a. Solid plate

Figure 9.   Effect of test entry on the Mach number deviations
with $\lambda = \lambda^*$, $\theta = 0$, and P_t = 1,600 psfa.

b. Porous wall
Figure 9. Concluded.
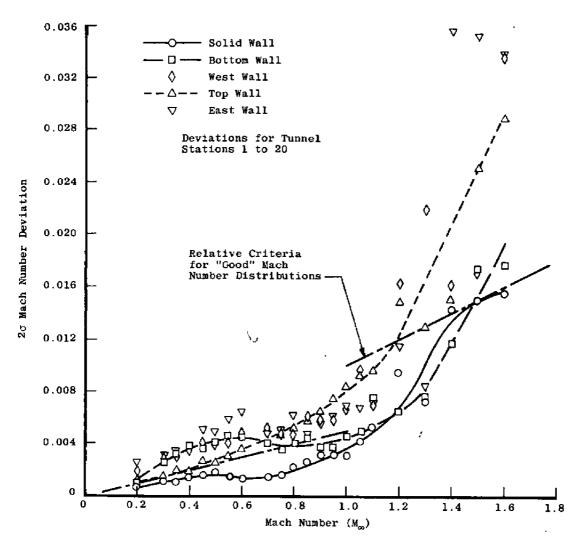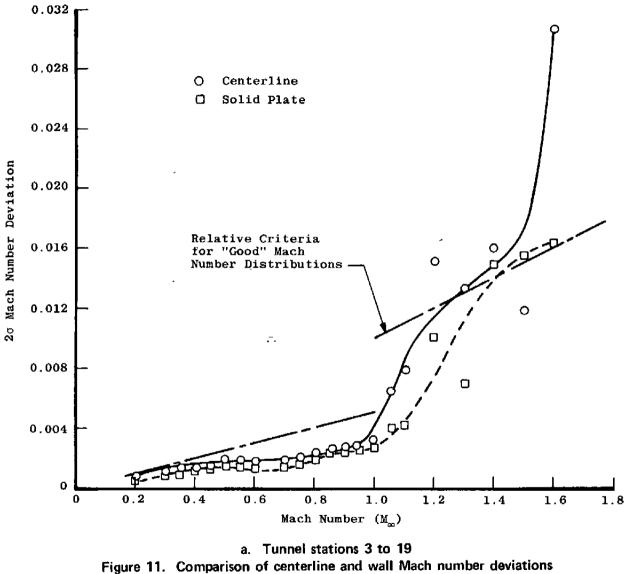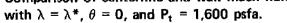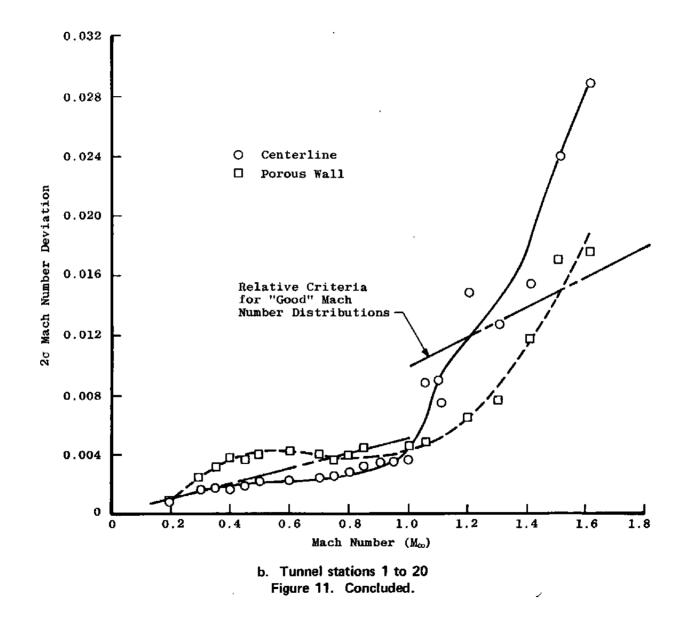
Figure 10. Mach number deviations for various wall Mach number distributions with λ = λ*, θ = 0, and P_t = 1,600 psfa.

a. Tunnel stations 3 to 19

Figure 11. Comparison of centerline and wall Mach number deviations
with $\lambda = \lambda^*$, $\theta = 0$, and $P_t = 1,600$ psfa.

b. Tunnel stations 1 to 20
Figure 11. Concluded.

a. Centerline pipe
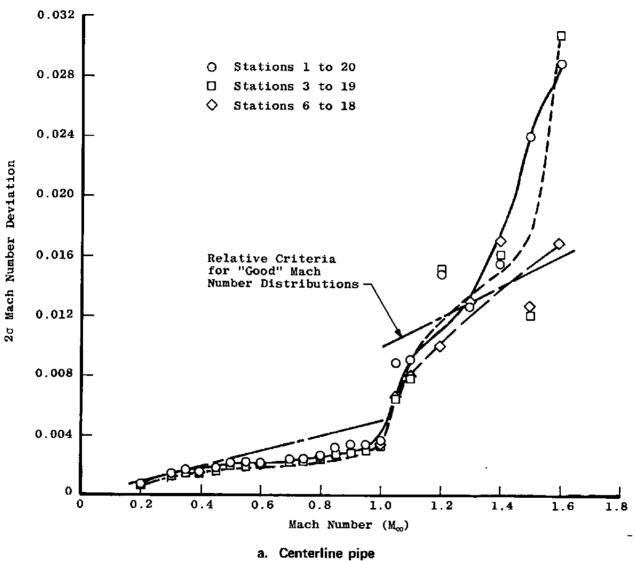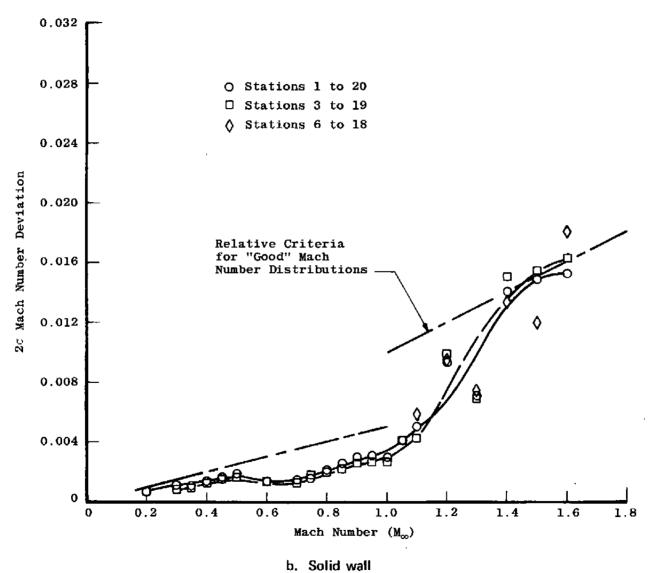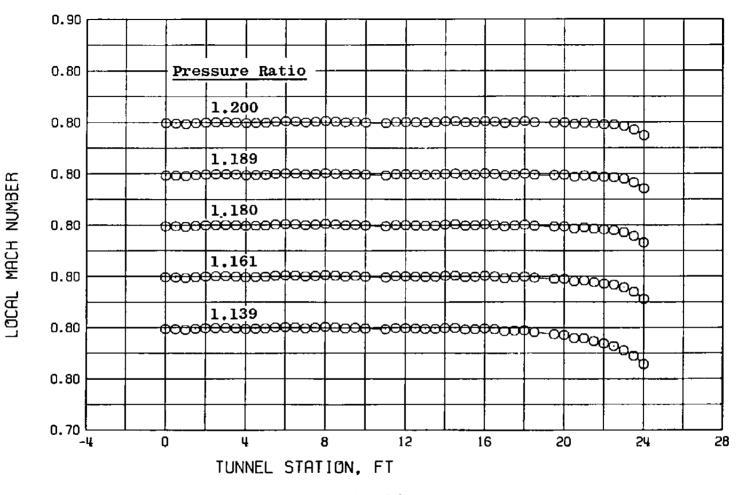
Figure 12. Effect of test region location on the Mach number deviations
with $\lambda = \lambda^*$, $\theta = 0$, and $P_t = 1,600$ psfa.

b. Solid wall

Figure 12. Concluded.
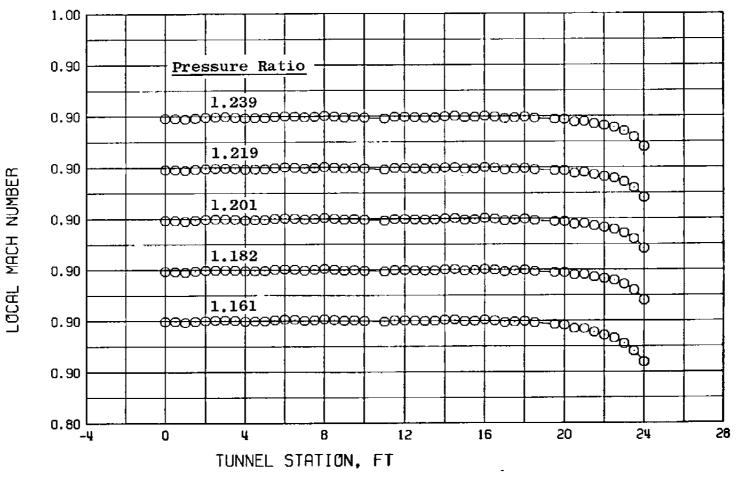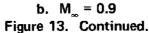
a. M_∞ = 0.8

Figure 13. Tunnel 16T centerline Mach number distributions for various tunnel pressure ratios with θ = 0 and P_t = 1,600 psfa.

b. $M_\infty = 0.9$
Figure 13. Continued.

c. $M_\infty = 1.0$
Figure 13. Continued.

d. $M_\infty = 1.1$
Figure 13. Continued.
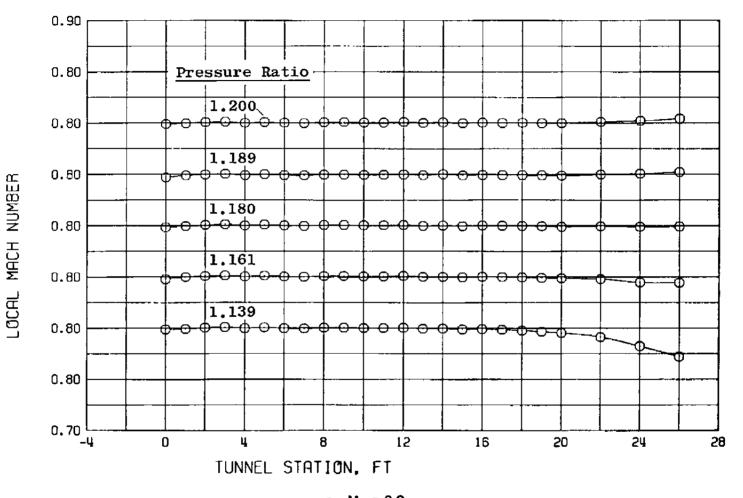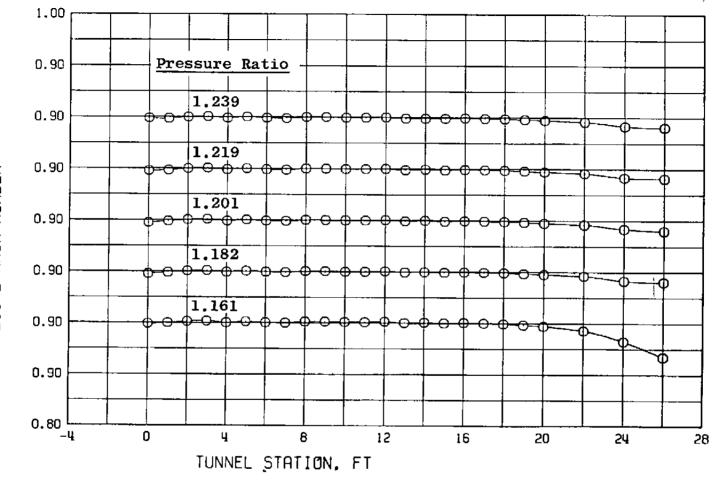
e. $M_\infty = 1.2$

Figure 13. Concluded.
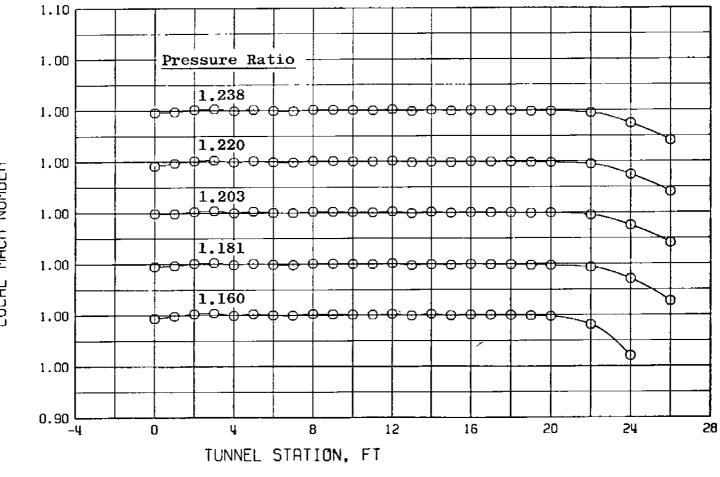
a. $M_\infty = 0.8$

Figure 14. Tunnel 16T wall Mach number distributions for various tunnel
pressure ratios with $\theta = 0$ and $P_t = 1,600$ psfa.
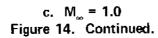
b. $M_\infty = 0.9$

Figure 14. Continued.

Pressure Ratio

1.238

1.220

1.203

1.181

1.160

LOCAL MACH NUMBER

TUNNEL STATION, FT

c. $M_\infty = 1.0$

Figure 14. Continued.

d. $M_\infty = 1.1$

Figure 14. Continued.

e. $M_\infty = 1.2$
Figure 14. Concluded.

a. Centerline pipe

Figure 15. Effect of tunnel pressure ratio on the Mach number deviations
for tunnel stations 6 to 18 with $\theta = 0$ and $P_t = 1,600$ psfa.

b. Solid plate
Figure 15. Concluded.

a. $M_\infty = 0.60$, centerline pipe

Figure 16. Effect of tunnel pressure ratio on the centerline and wall Mach number distributions at $M_\infty \leqslant 0.75$ with $\theta = 0$ and $P_t = 1,600$ psfa.

b. $M_\infty = 0.70$, centerline pipe
Figure 16. Continued.

c. $M_\infty = 0.70$, solid wall
Figure 16. Continued.

Note: 2σ for Stations 6 to 18

d. $M_\infty = 0.75$, centerline pipe
Figure 16. Concluded.
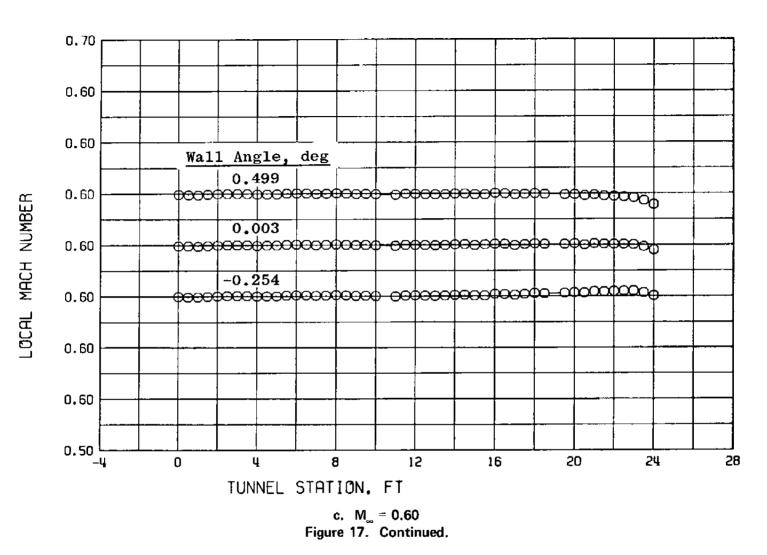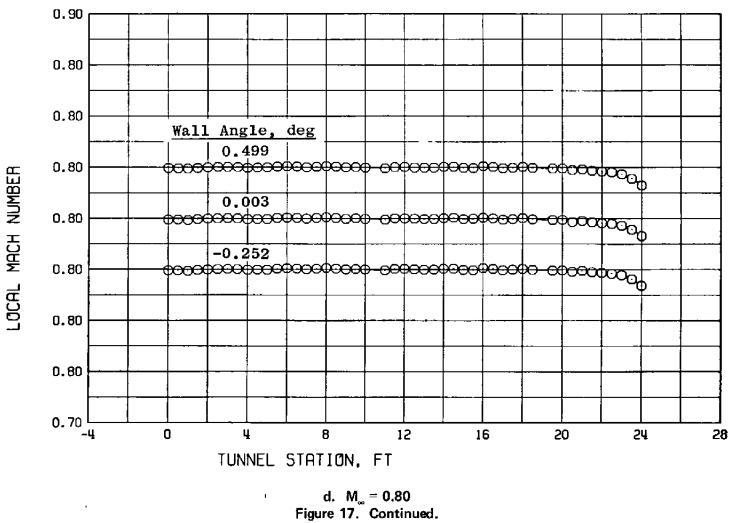
a. $M_\infty = 0.20$

Figure 17. Tunnel 16T centerline Mach number distributions for various test section wall angles with $\lambda = \lambda^*$ and $P_t = 1,600$ psfa.

b. $M_\infty = 0.40$
Figure 17. Continued.

c. $M_\infty = 0.60$
Figure 17. Continued.

d. $M_\infty = 0.80$
Figure 17. Continued.

e. $M_\infty = 1.00$
Figure 17. Continued.

f. $M_\infty = 1.20$
Figure 17. Continued.
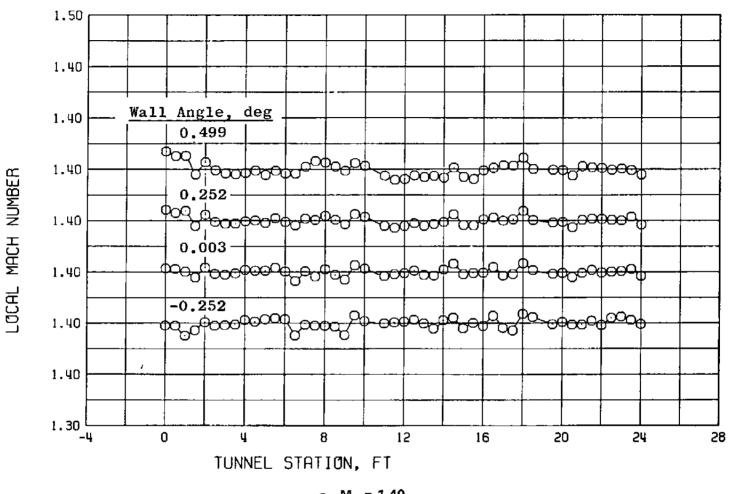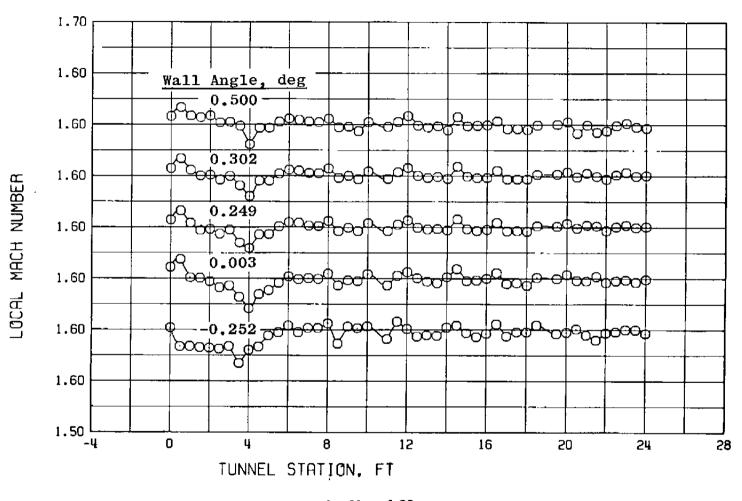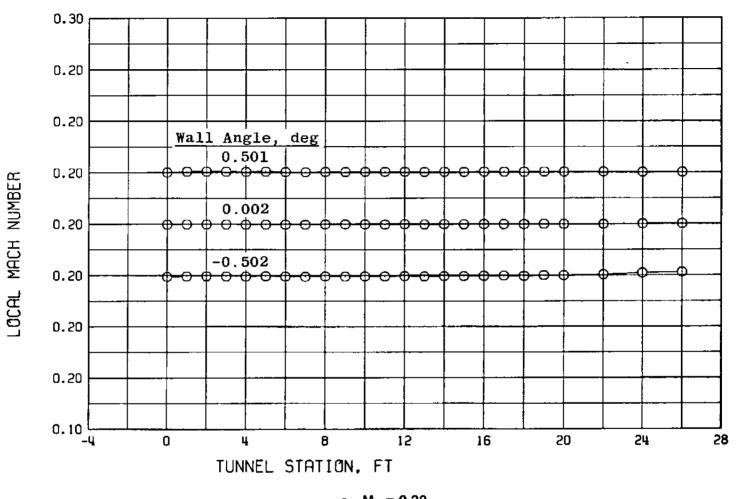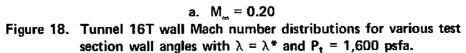
g. $M_\infty = 1.40$
Figure 17. Continued.
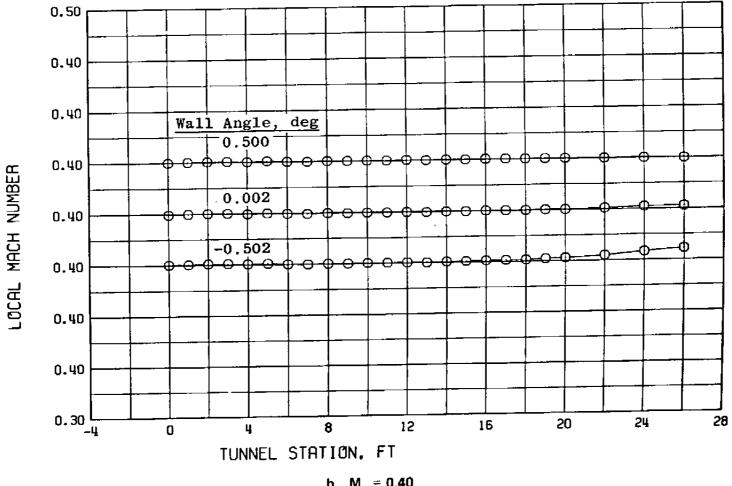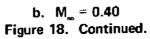
h. $M_\infty = 1.60$

Figure 17. Concluded.

LOCAL MACH NUMBER

TUNNEL STATION, FT

Wall Angle, deg

0.501

0.002

-0.502

0.30
0.20
0.20
0.20
0.20
0.20
0.20
0.20
0.10

-4   0   4   8   12   16   20   24   28

a. $M_\infty = 0.20$

Figure 18. Tunnel 16T wall Mach number distributions for various test
section wall angles with $\lambda = \lambda^*$ and $P_t = 1,600$ psfa.

b. $M_\infty = 0.40$
Figure 18. Continued.

c. $M_\infty = 0.60$

Figure 18. Continued.

d. $M_\infty = 0.80$

Figure 18. Continued.
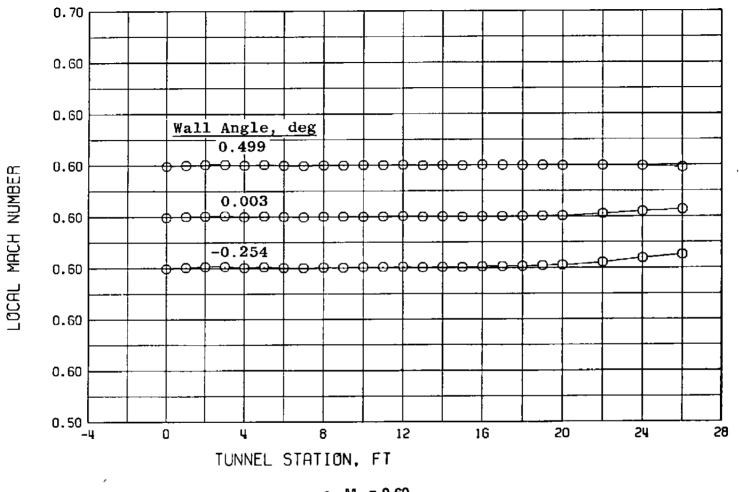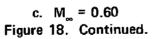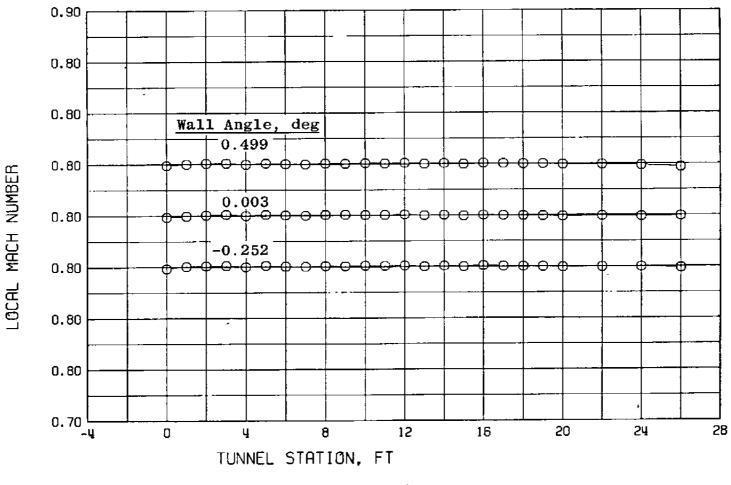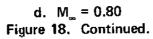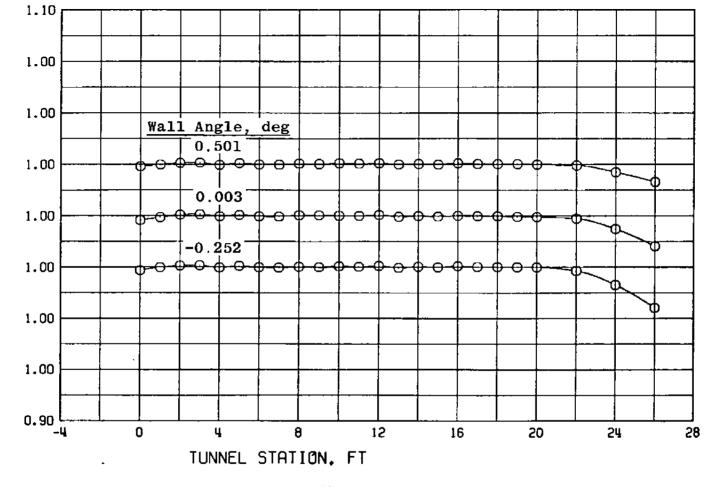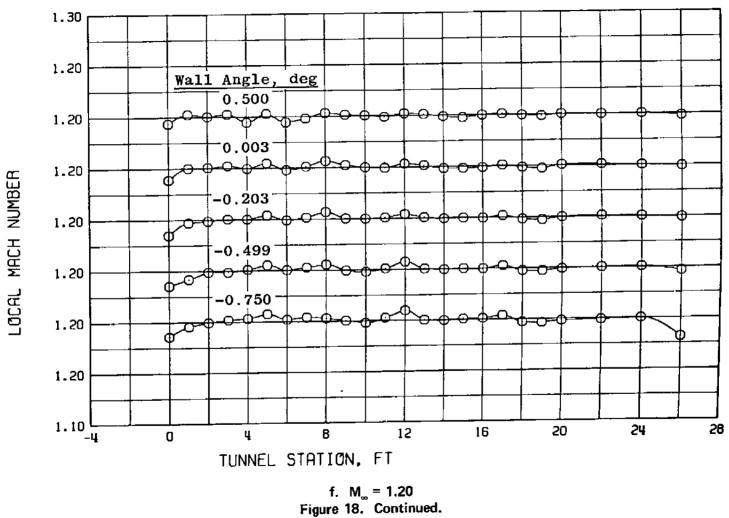
e. $M_\infty = 1.00$
Figure 18. Continued.

f. $M_\infty = 1.20$
Figure 18. Continued.
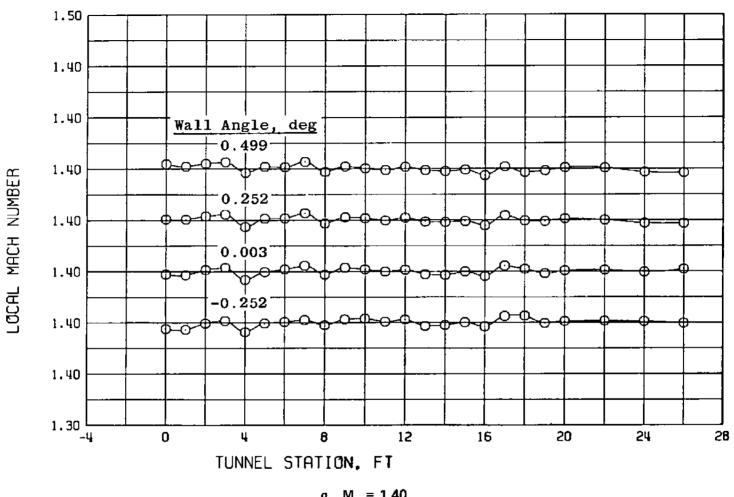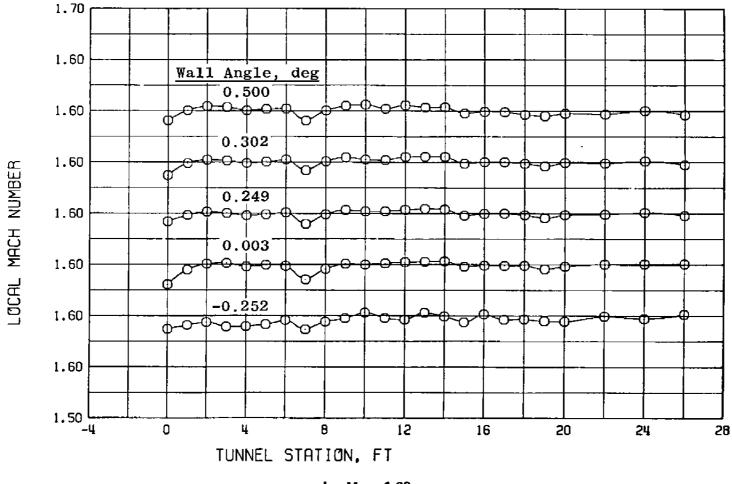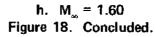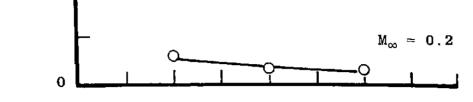
g. $M_\infty = 1.40$
Figure 18. Continued.

h. $M_\infty = 1.60$

Figure 18. Concluded.
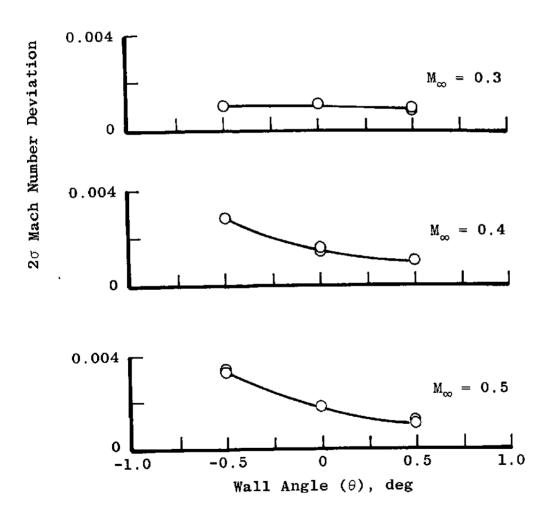
$$\theta* = 0$$
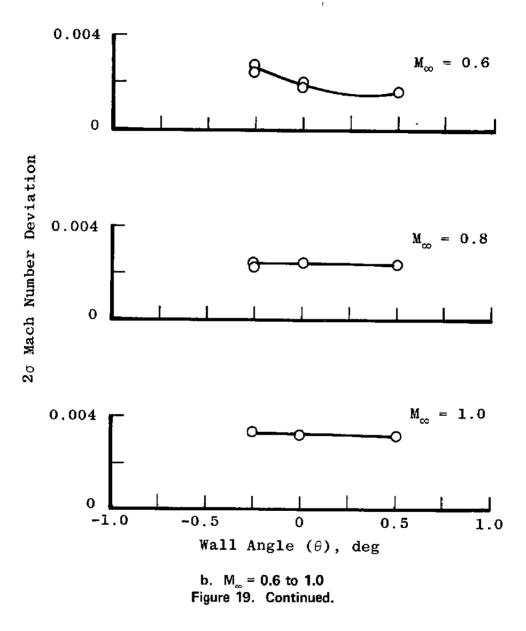

a. M_∞ = 0.2 to 0.5

Figure 19. Effect of test section wall angle on the centerline Mach number deviations for tunnel stations 6 to 18 with $\lambda = \lambda*$ and P_t = 1,600 psfa.

$\theta* = 0$

b. $M_\infty = 0.6$ to 1.0
Figure 19. Continued.
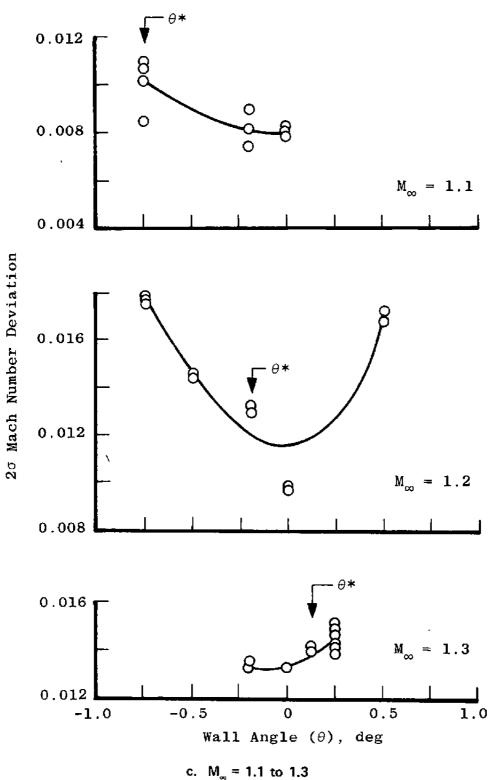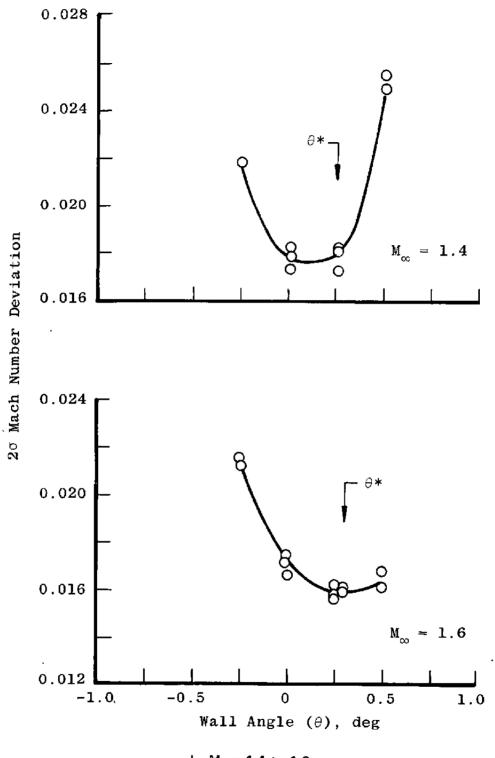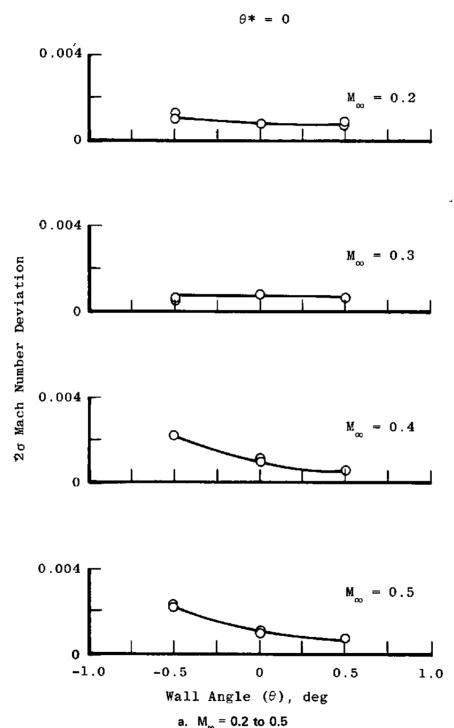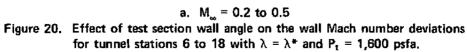
c. M_∞ = 1.1 to 1.3
Figure 19. Continued.
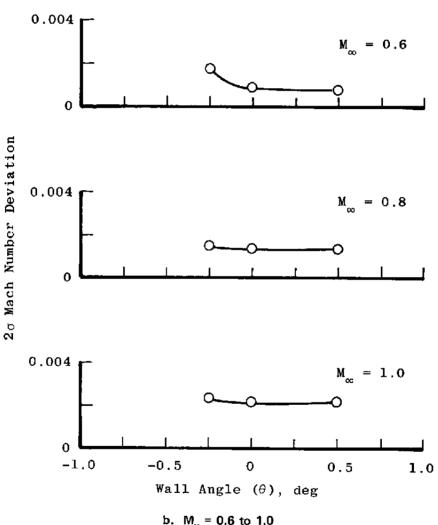
d. M_∞ = 1.4 to 1.6
Figure 19. Concluded.

a. M_∞ = 0.2 to 0.5

Figure 20. Effect of test section wall angle on the wall Mach number deviations for tunnel stations 6 to 18 with $\lambda = \lambda^*$ and P_t = 1,600 psfa.

$\theta* = 0$
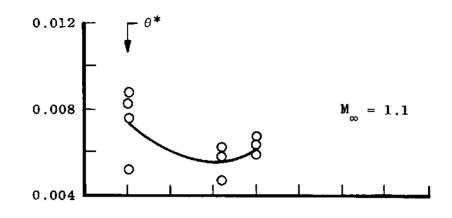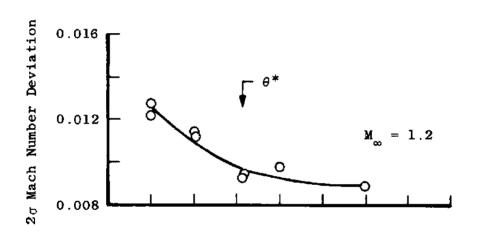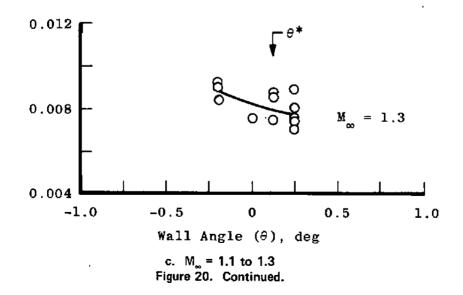
b. $M_\infty = 0.6$ to 1.0
Figure 20. Continued.

c. M_{∞} = 1.1 to 1.3
Figure 20. Continued.
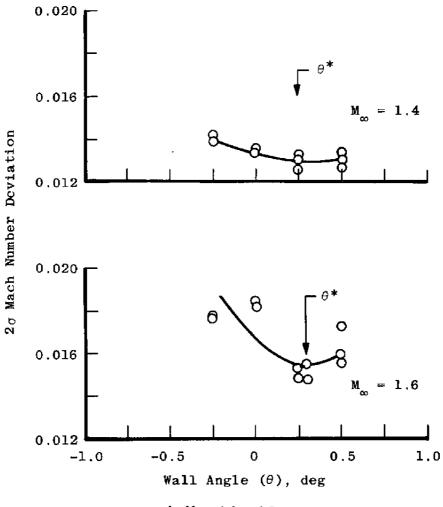
d. M_∞ = 1.4 to 1.6
Figure 20. Concluded.

a. $M_\infty = 0.20$
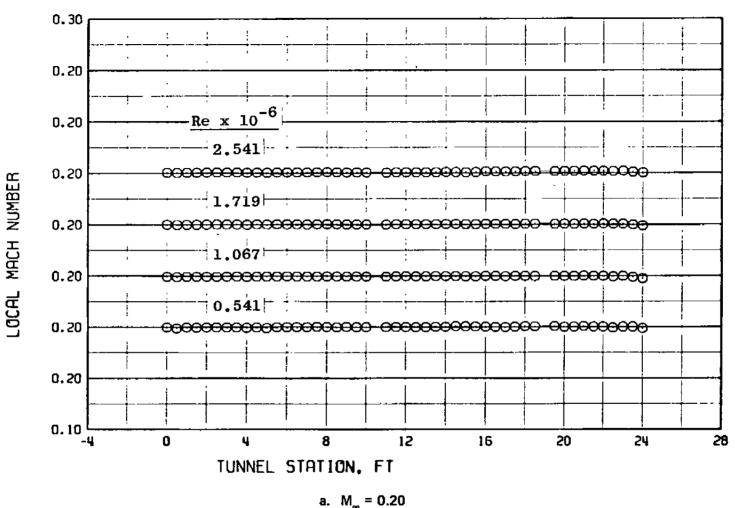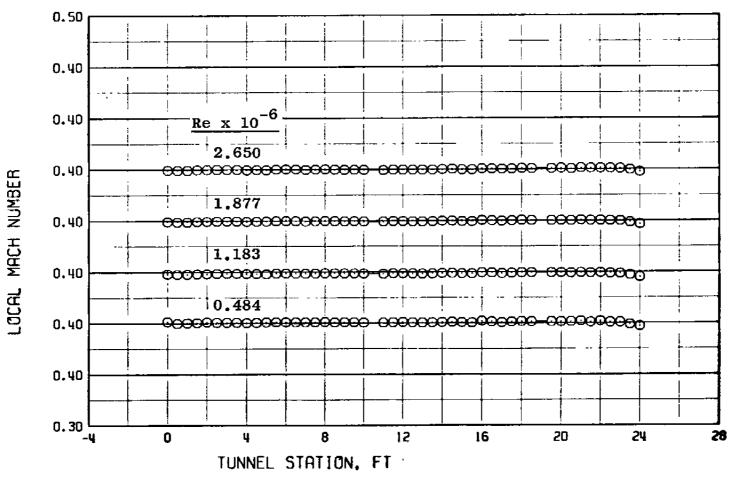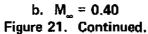
Figure 21. Tunnel 16T centerline Mach number distributions for various
Reynolds numbers with $\lambda = \lambda^*$ and $\theta = 0$.

b. $M_\infty = 0.40$
Figure 21. Continued.
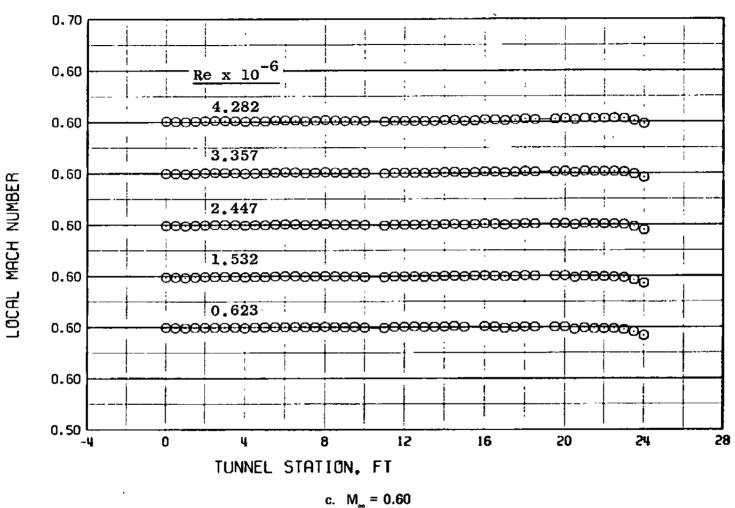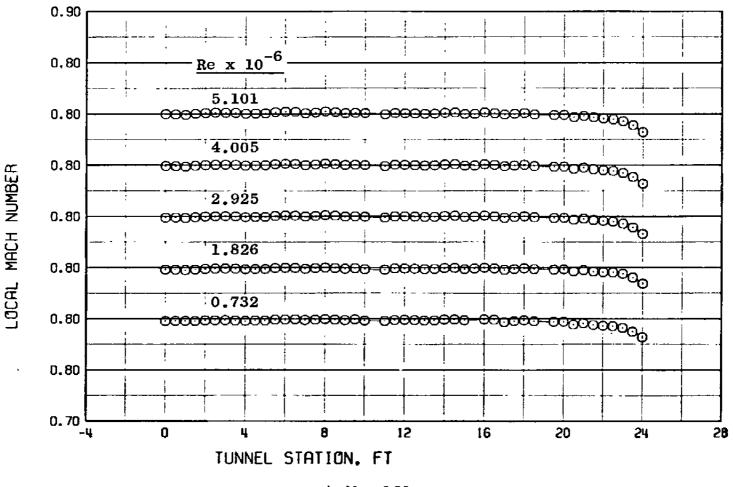
c. $M_\infty = 0.60$
Figure 21. Continued.

d. $M_\infty = 0.80$
Figure 21. Continued.

e. $M_\infty = 1.00$
Figure 21. Continued.

f. $M_\infty = 1.20$

Figure 21. Continued.

g. $M_\infty = 1.40$
Figure 21. Continued.

h. $M_\infty = 1.60$
Figure 21. Concluded.

LOCAL MACH NUMBER

0.30

0.20

0.20

0.20

0.20

0.20

0.20

0.20

0.10

$\underline{\text{Re} \times 10^{-6}}$

2.541

1.719

1.067

0.541

-4   0   4   8   12   16   20   24   28

TUNNEL STATION, FT

a. $M_\infty = 0.20$

Figure 22. Tunnel 16T wall Mach number distributions for various
Reynolds numbers with $\lambda = \lambda^*$ and $\theta = 0$.

b. $M_\infty = 0.40$

Figure 22. Continued.
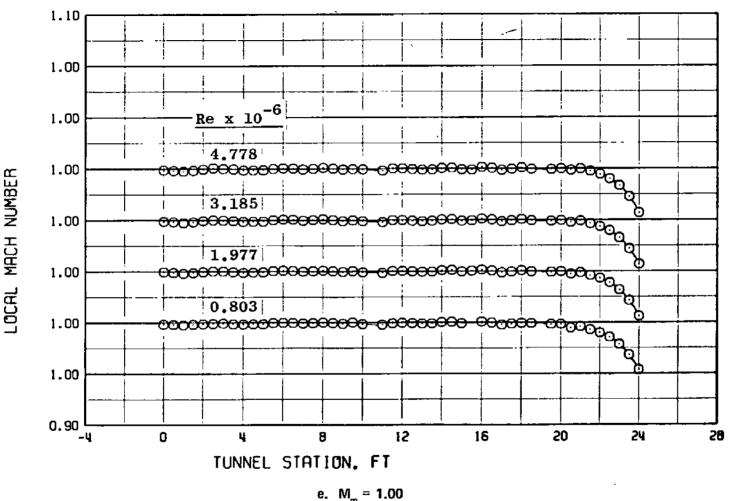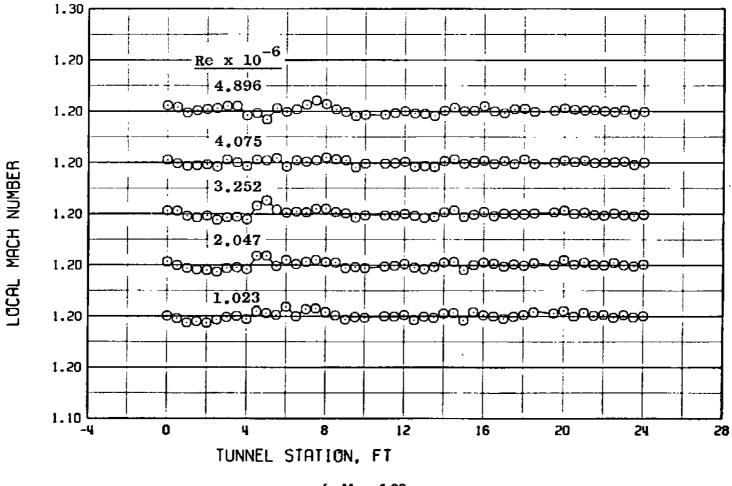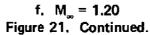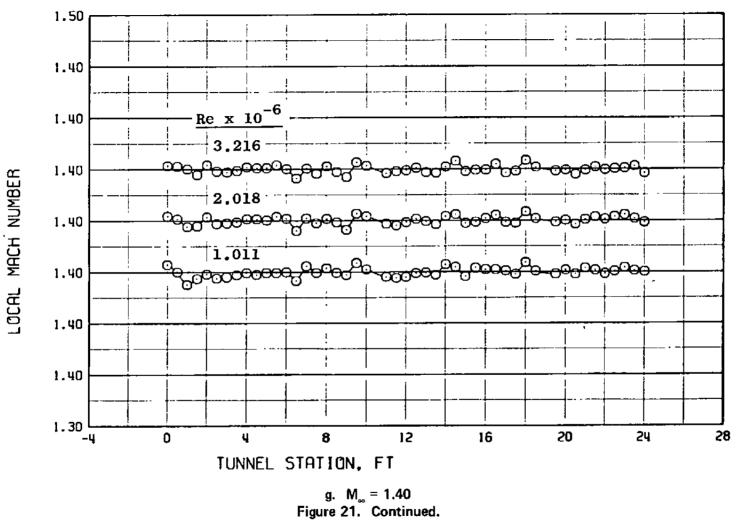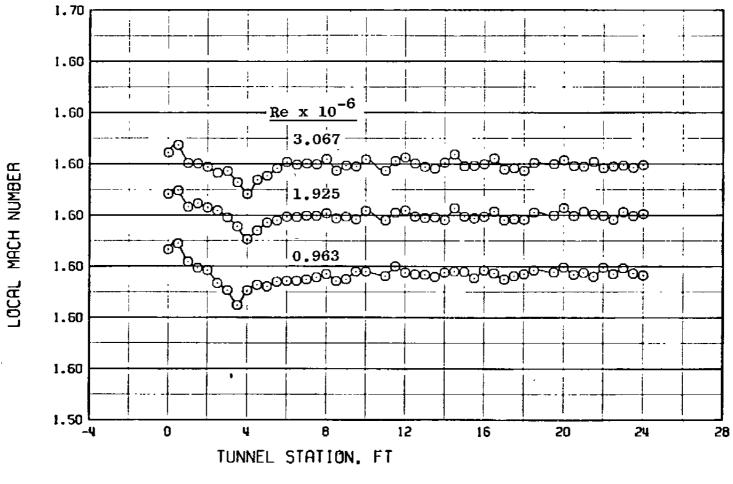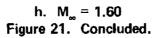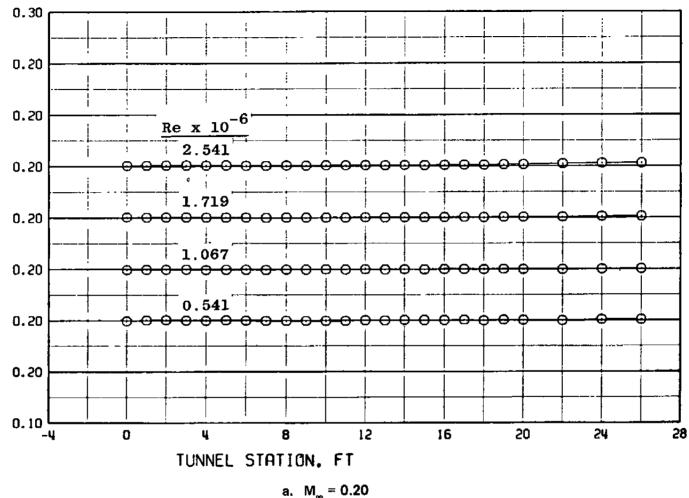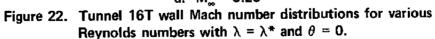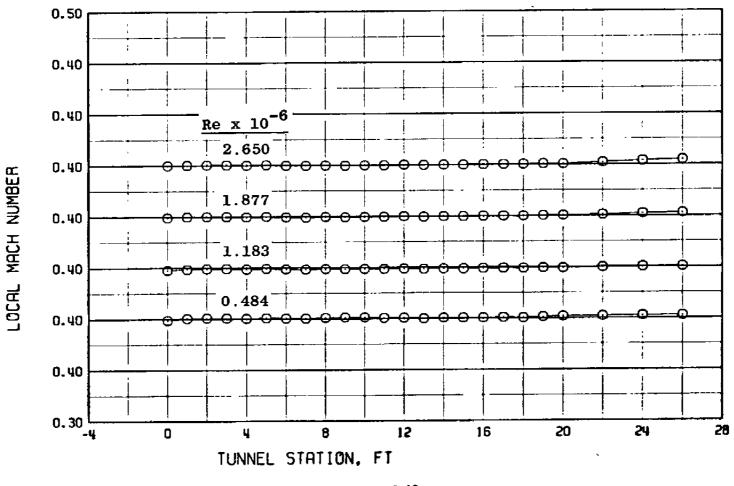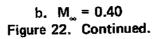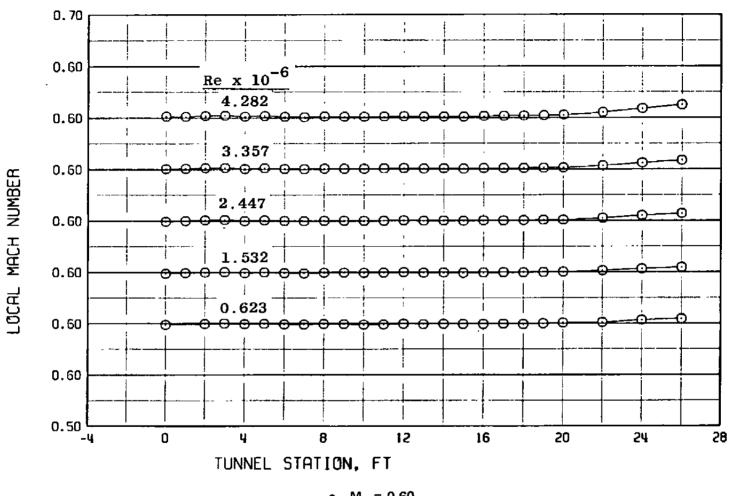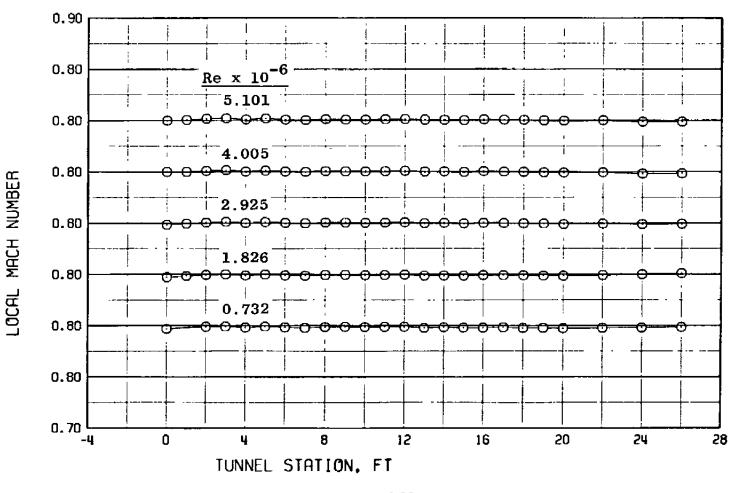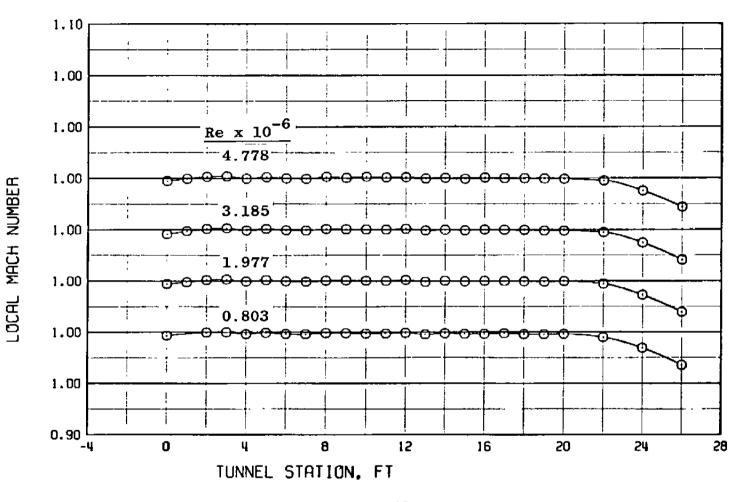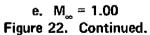
c. $M_\infty = 0.60$
Figure 22. Continued.

d. $M_\infty = 0.80$

Figure 22. Continued.
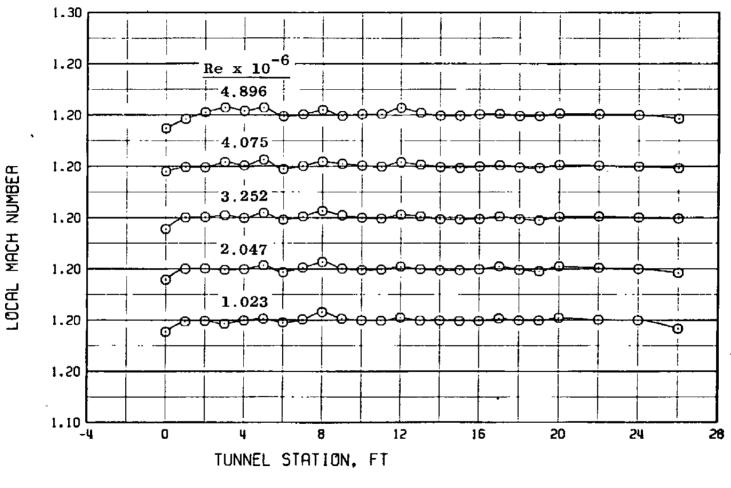
e. $M_\infty = 1.00$
Figure 22. Continued.
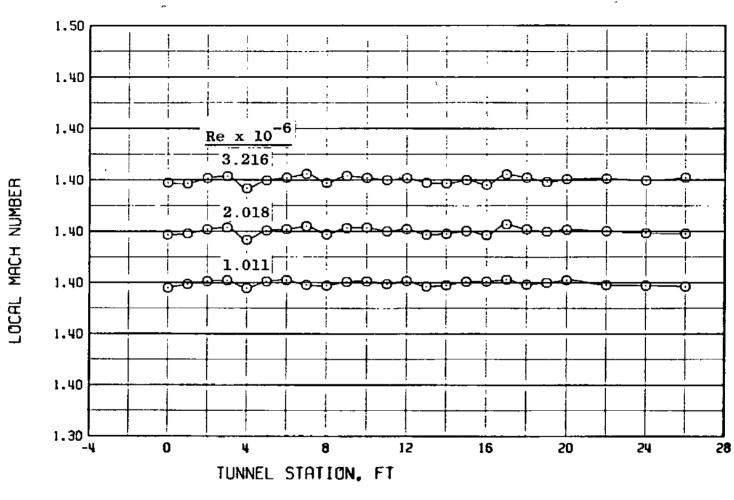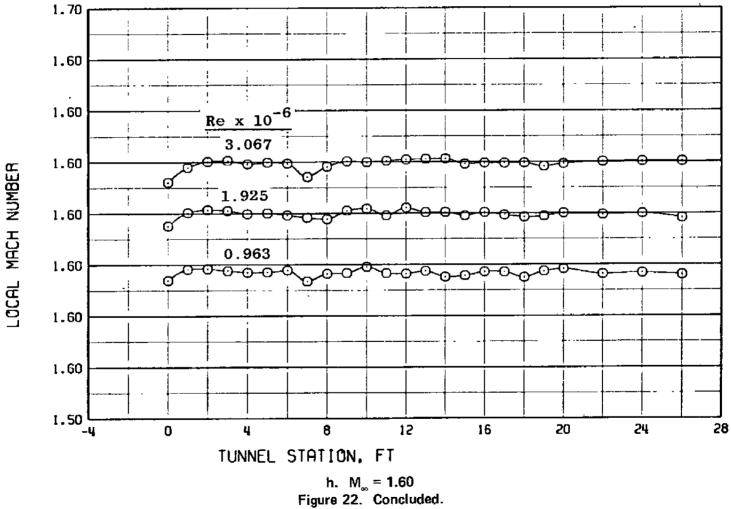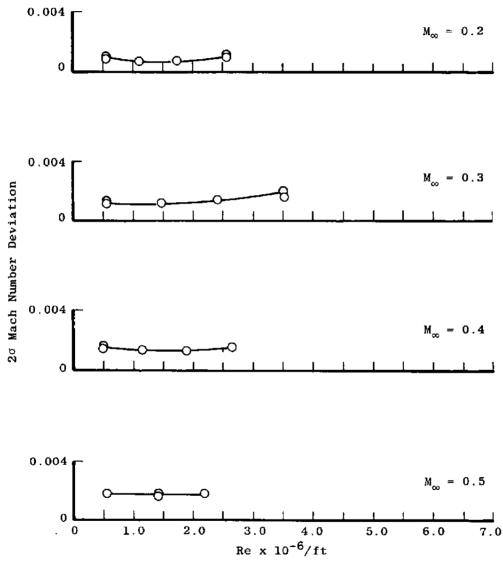
f. $M_\infty = 1.20$
Figure 22. Continued.

g. $M_\infty = 1.40$

Figure 22. Continued.

h. $M_\infty = 1.60$

Figure 22. Concluded.
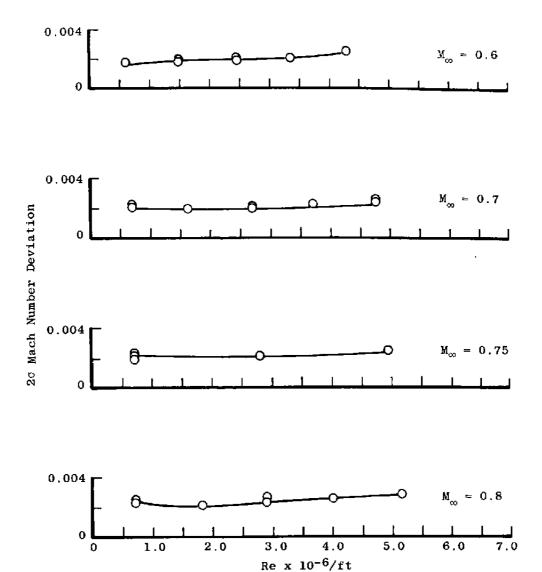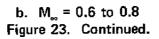
a. M_∞ = 0.2 to 0.5

Figure 23. Effect of Reynolds number on the centerline Mach number deviations for tunnel stations 6 to 18 with $\lambda = \lambda^*$ and $\theta = 0$.

b. M_∞ = 0.6 to 0.8
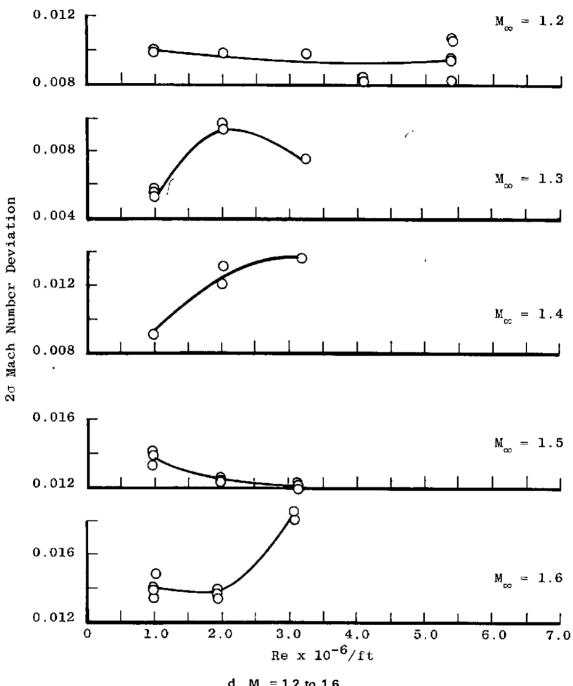Figure 23. Continued.

c. $M_\infty = 0.85$ to 1.1
Figure 23. Continued.

128
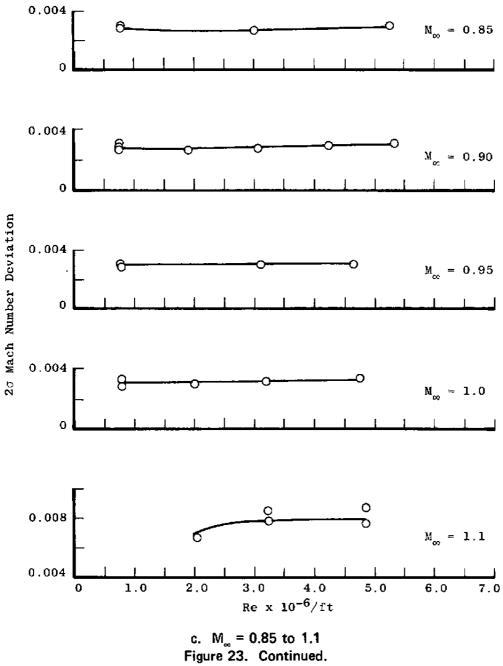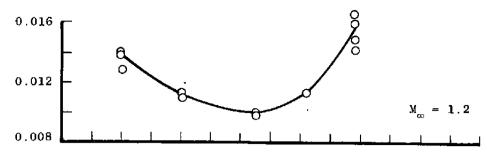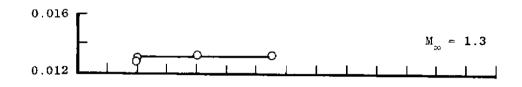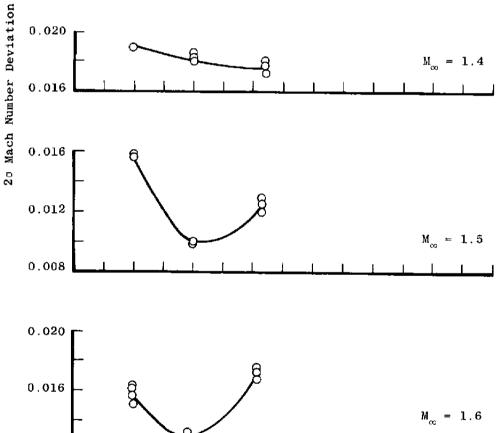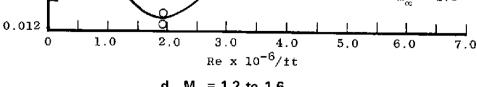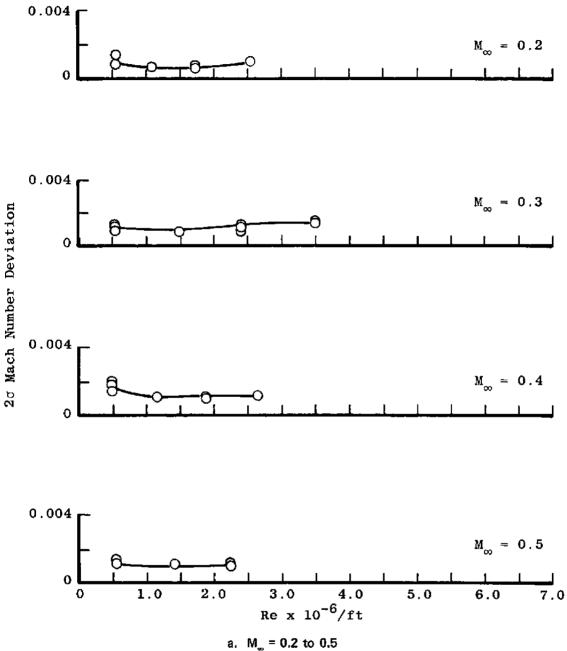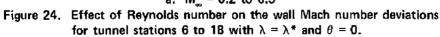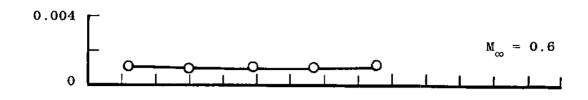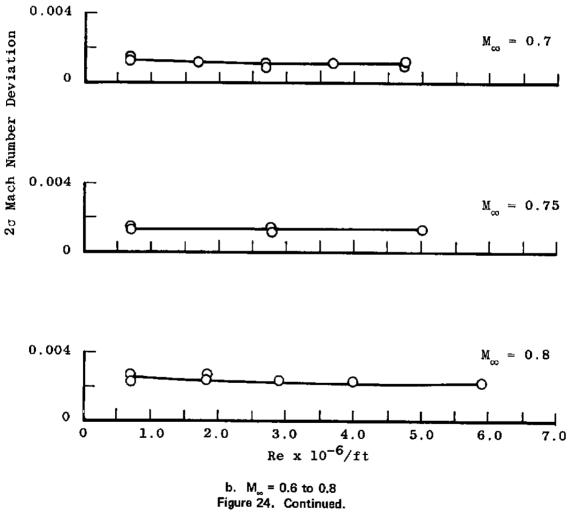
d. M_∞ = 1.2 to 1.6
Figure 23. Concluded.

a. M∞ = 0.2 to 0.5
Figure 24. Effect of Reynolds number on the wall Mach number deviations
for tunnel stations 6 to 18 with $\lambda = \lambda^*$ and $\theta = 0$.

b. M_∞ = 0.6 to 0.8
Figure 24. Continued.

c. M_∞ = 0.85 to 1.1
Figure 24. Continued.

132
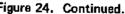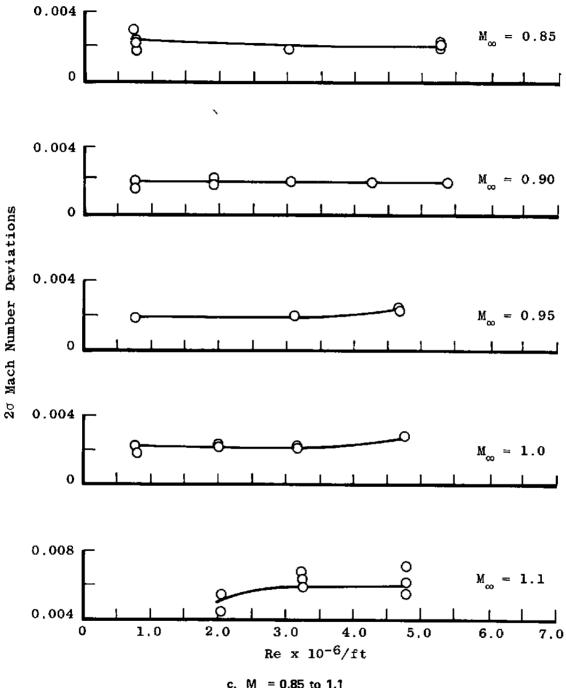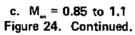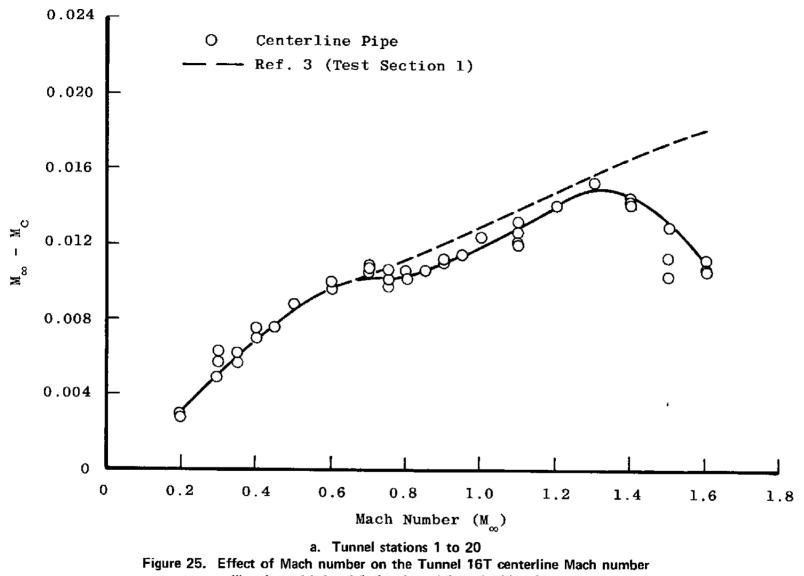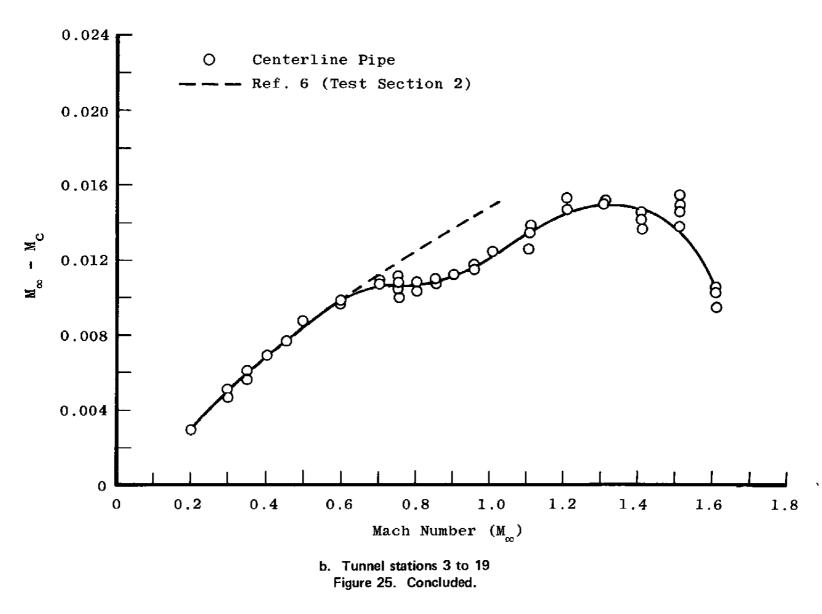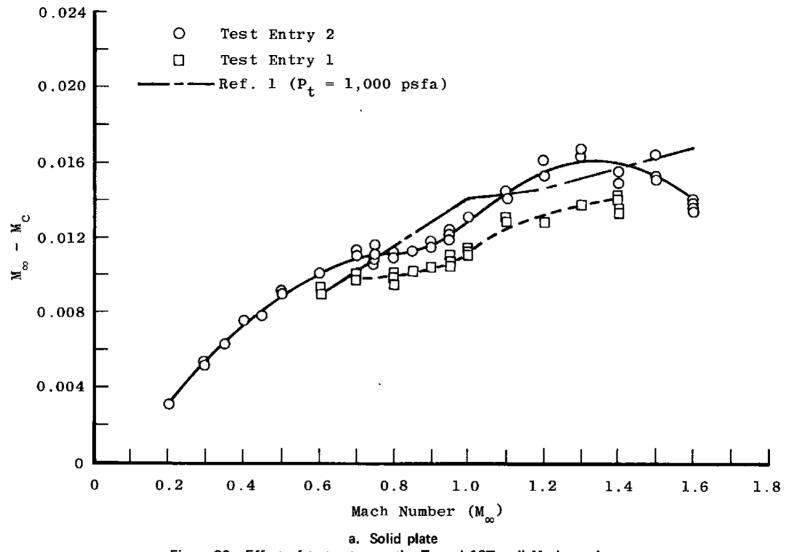
d. $M_\infty = 1.2$ to 1.6
Figure 24. Concluded.

a. Tunnel stations 1 to 20

Figure 25. Effect of Mach number on the Tunnel 16T centerline Mach number
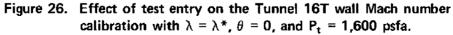calibration with $\lambda = \lambda^*$, $\theta = 0$, and $P_t = 1,600$ psfa.

b. Tunnel stations 3 to 19
Figure 25. Concluded.

a. Solid plate
Figure 26. Effect of test entry on the Tunnel 16T wall Mach number
calibration with $\lambda = \lambda*$, $\theta = 0$, and $P_t = 1,600$ psfa.

b. Porous wall
Figure 26. Concluded.

a. Tunnel stations 3 to 19

Figure 27. Comparison of centerline and wall Mach number calibrations
with $\lambda = \lambda^*$, $\theta = 0$, and $P_t = 1,600$ psfa.

b. Tunnel stations 1 to 20
Figure 27. Continued.
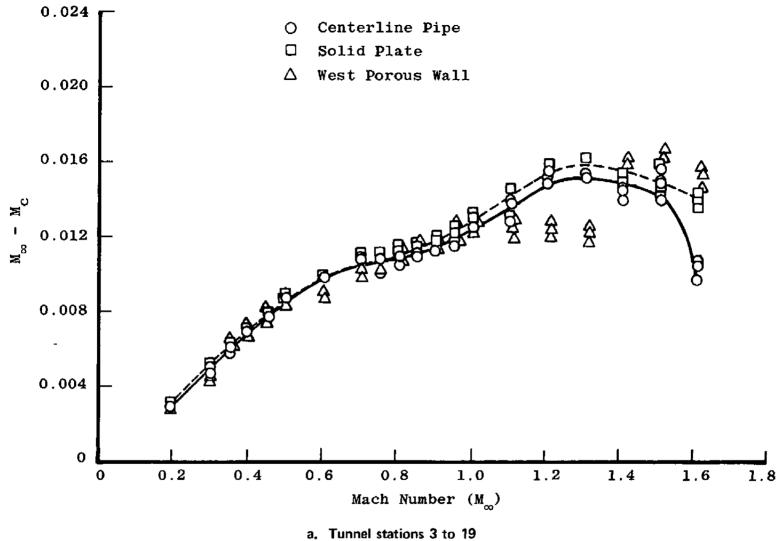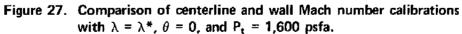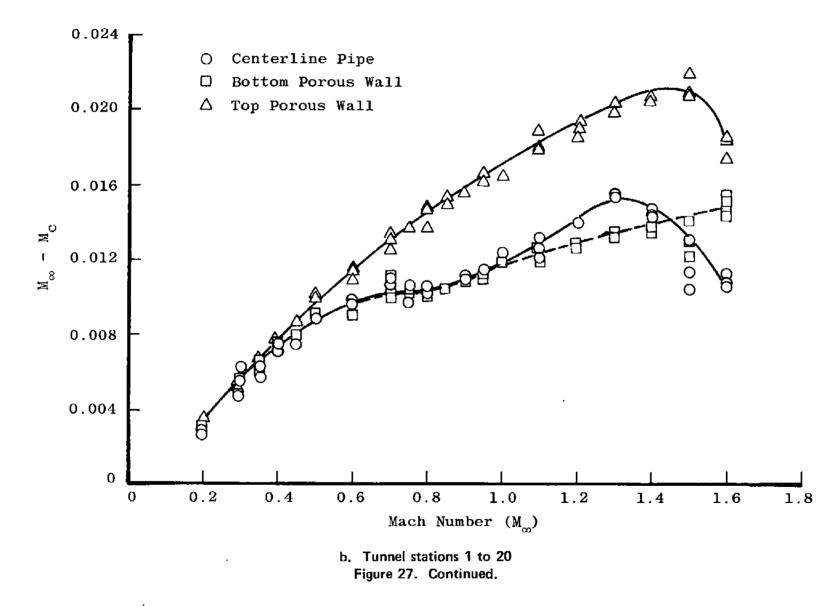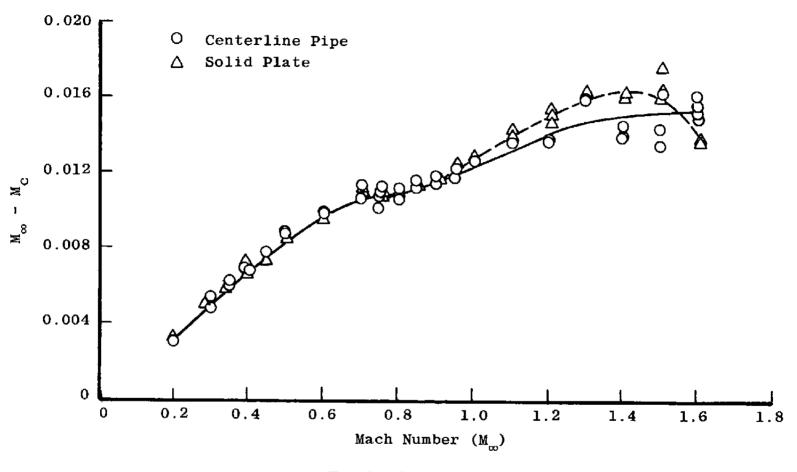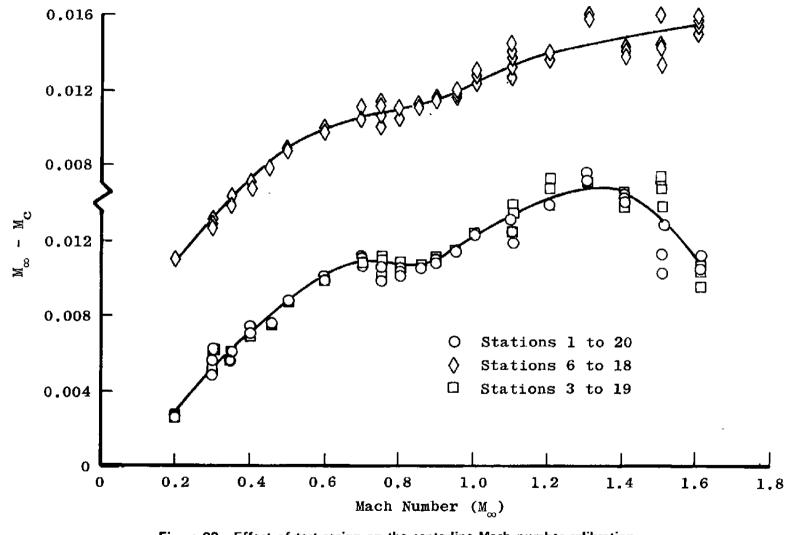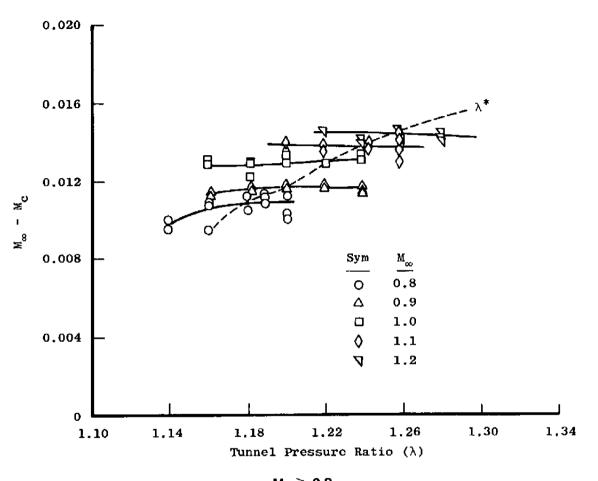
c. Tunnel stations 6 to 18
Figure 27. Concluded.
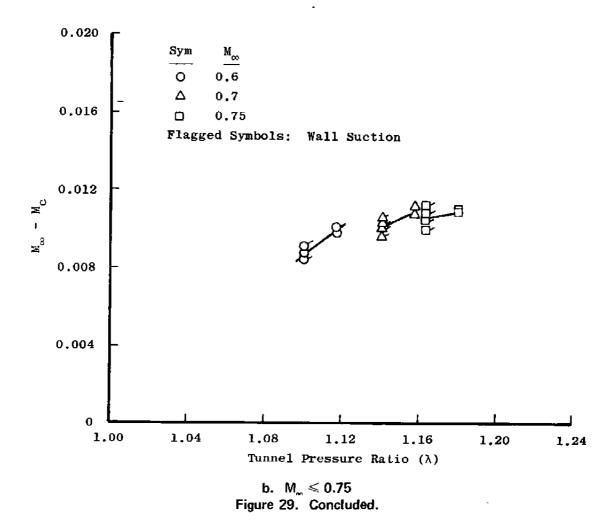
Figure 28. Effect of test region on the centerline Mach number calibration with $\lambda = \lambda^*$, $\theta = 0$, and $P_t = 1,600$ psfa.

a. $M_\infty \geqslant 0.8$

Figure 29. Effect of tunnel pressure ratio on the centerline Mach number
calibration with $\theta = 0$ and $P_t = 1,600$ psfa.

b. $M_\infty \leqslant 0.75$
Figure 29. Concluded.

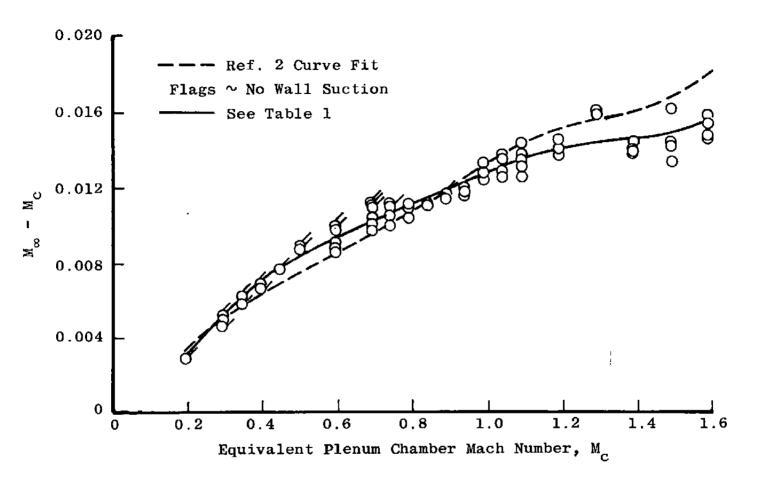AEDC-TR-78-60

Figure 30. Tunnel 16T Mach number calibration with $\lambda = \lambda^*$, $\theta = 0$, and $P_t = 1,600$ psfa.
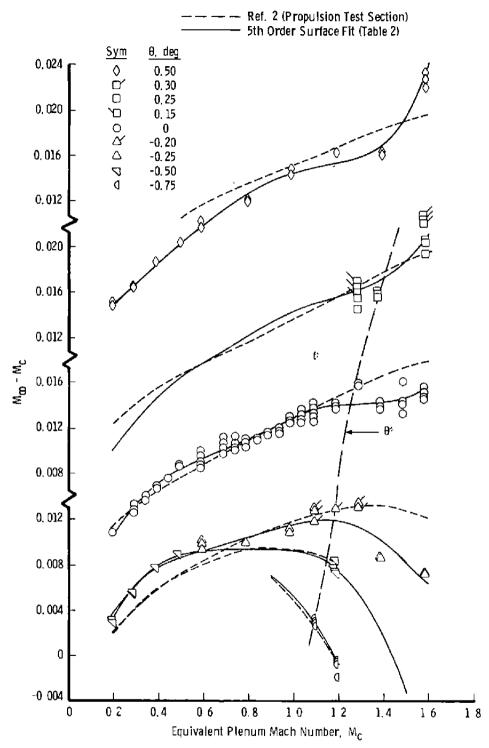
Figure 31. Tunnel 16T Mach number calibration for various test section wall angles with λ = λ* and P_t = 1,600 psfa.
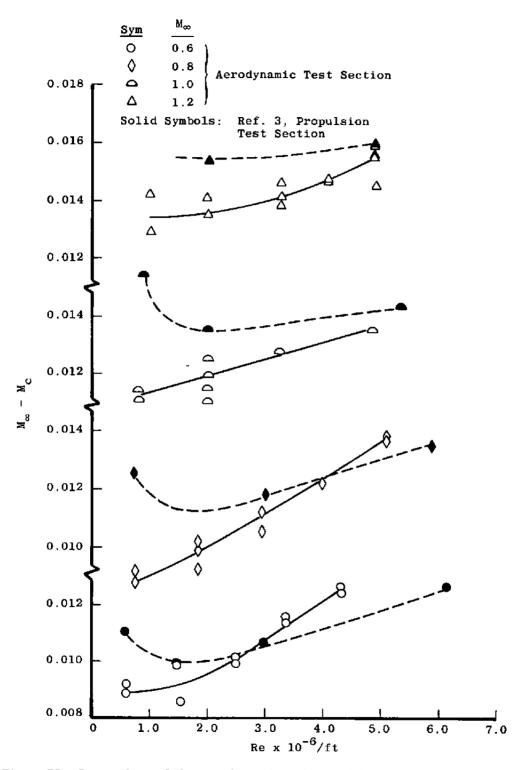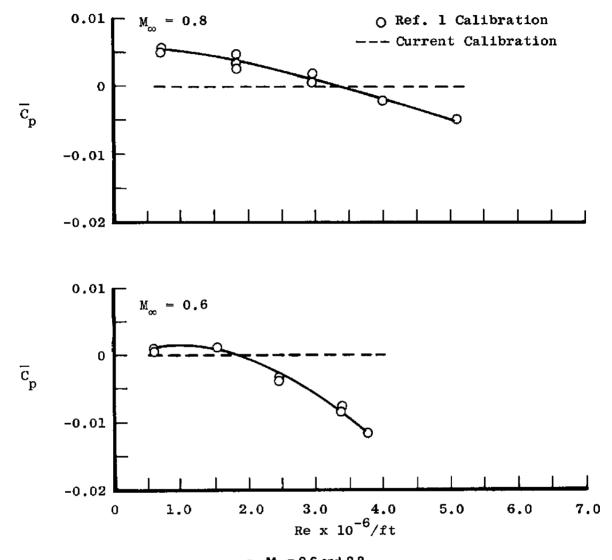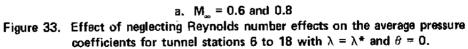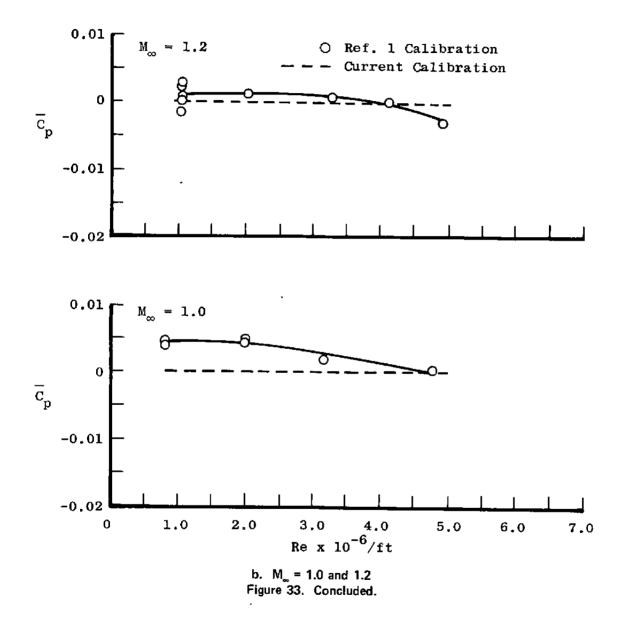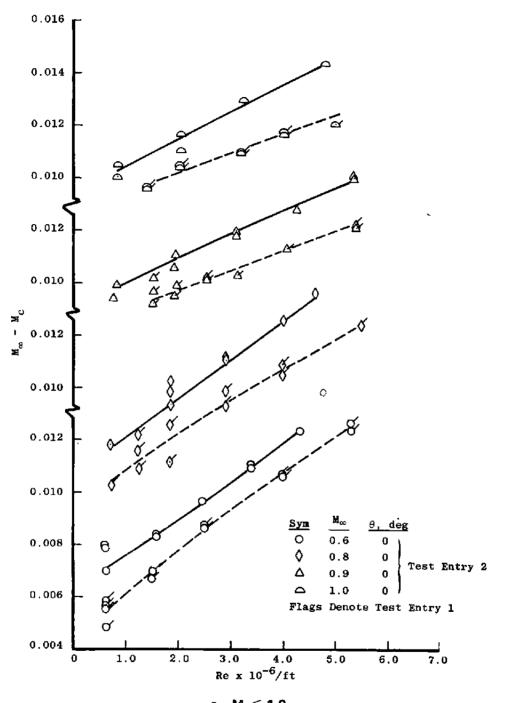
Figure 32. Comparison of the aerodynamic and propulsion test section centerline Mach number calibrations with $\lambda = \lambda^*$ and $\theta = 0$.

a. M_∞ = 0.6 and 0.8

Figure 33. Effect of neglecting Reynolds number effects on the average pressure
coefficients for tunnel stations 6 to 18 with $\lambda = \lambda^*$ and $\theta = 0$.

b. $M_\infty = 1.0$ and 1.2
Figure 33. Concluded.
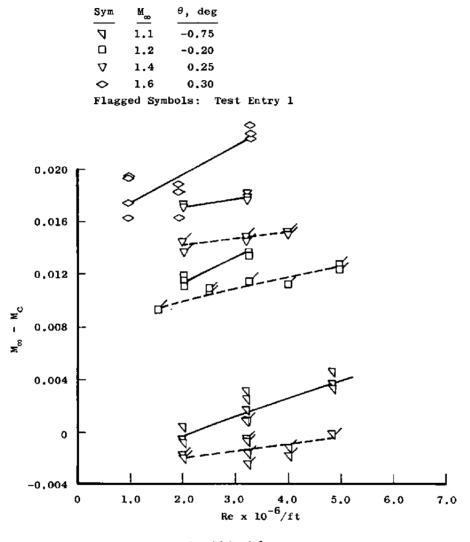
a. $M_\infty \leqslant 1.0$

Figure 34. Tunnel 16T wall Mach number calibration for various Reynolds numbers with $\lambda = \lambda^*$ and $\theta = \theta^*$.

Sym	M_∞	θ, deg
◁	1.1	−0.75
◻	1.2	−0.20
▽	1.4	0.25
◇	1.6	0.30

Flagged Symbols: Test Entry 1

b. M ⩾ 1.0

Figure 34. Concluded.

a. $0.2 \leqslant M_\infty \leqslant 0.5$
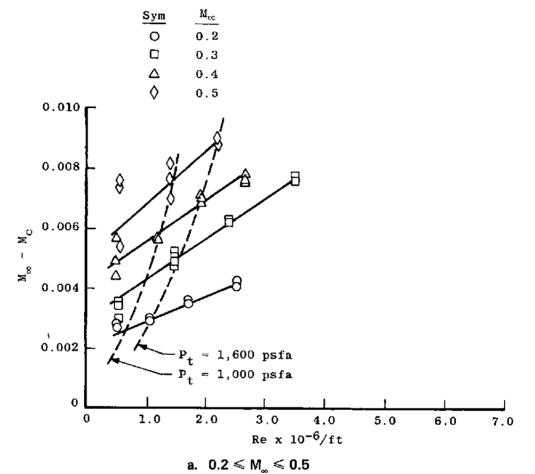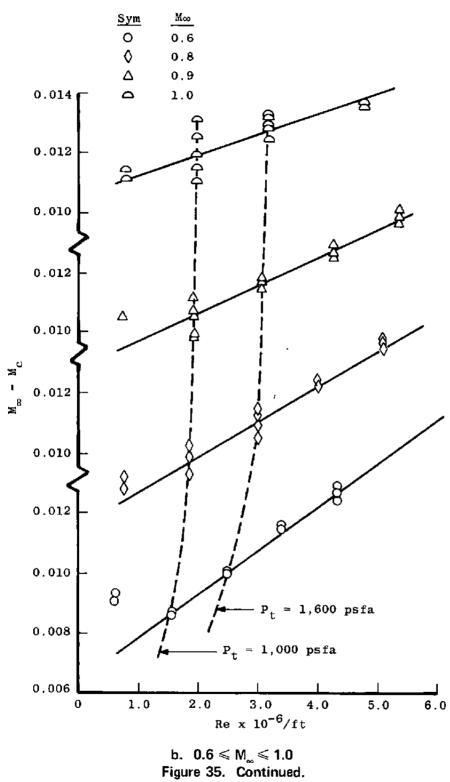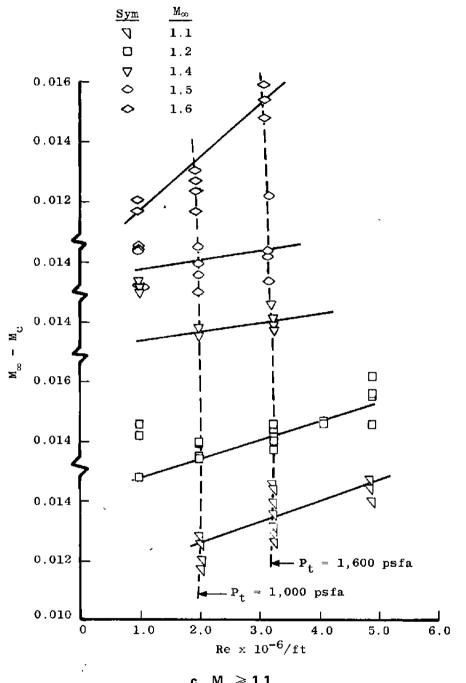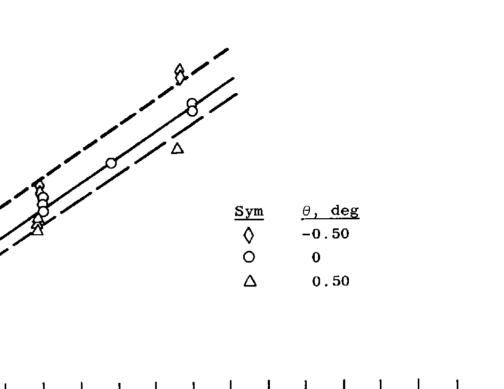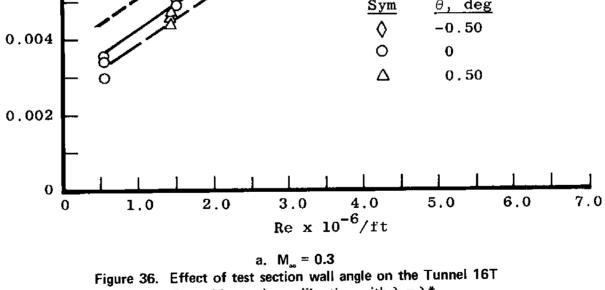
Figure 35. Tunnel 16T centerline Mach number calibration for various
Reynolds numbers with $\lambda = \lambda^*$ and $\theta = 0$.

b. $0.6 \leqslant M_\infty \leqslant 1.0$
Figure 35. Continued.

c. $M_\infty \geqslant 1.1$
Figure 35. Concluded.

153

a. $M_\infty = 0.3$

Figure 36. Effect of test section wall angle on the Tunnel 16T
Reynolds number calibration with $\lambda = \lambda^*$.

b. $M_\infty = 0.6$
Figure 36. Continued.
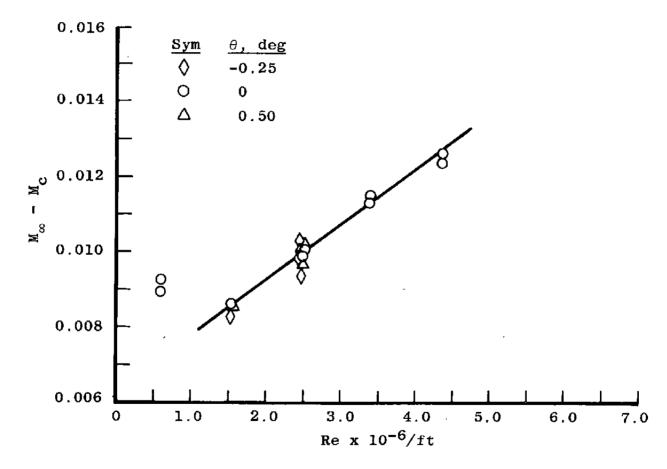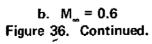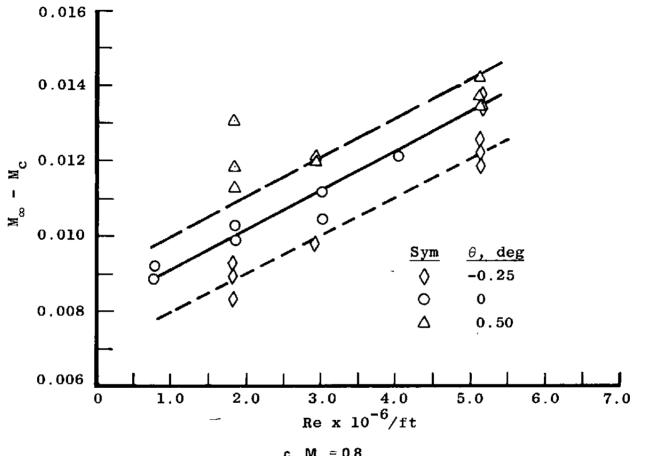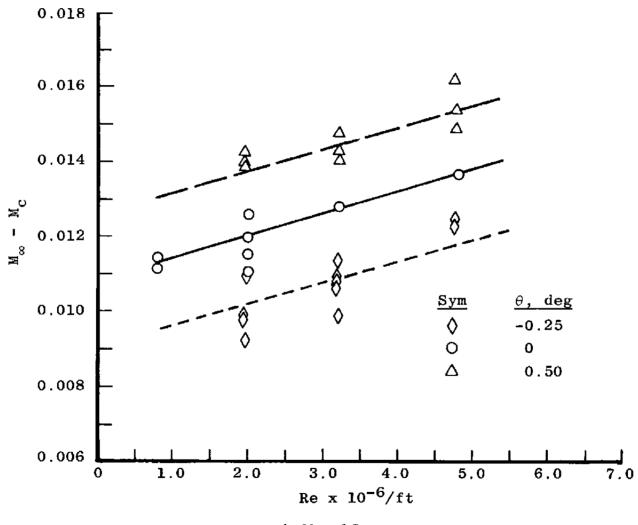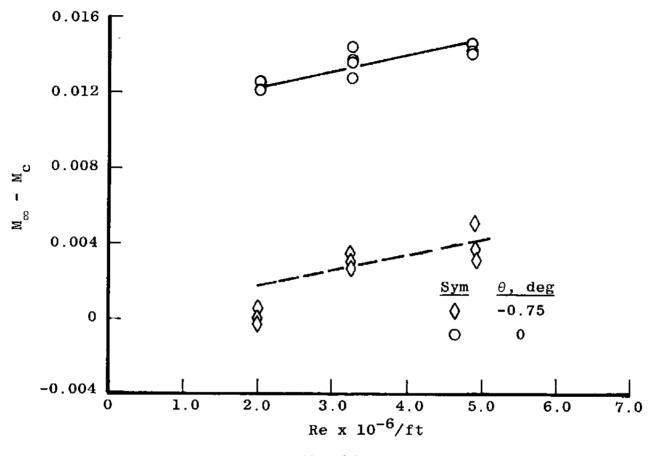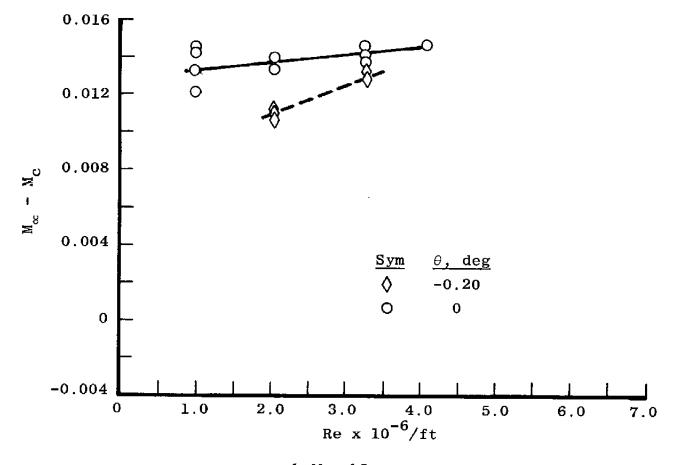
c. $M_\infty = 0.8$

Figure 36. Continued.
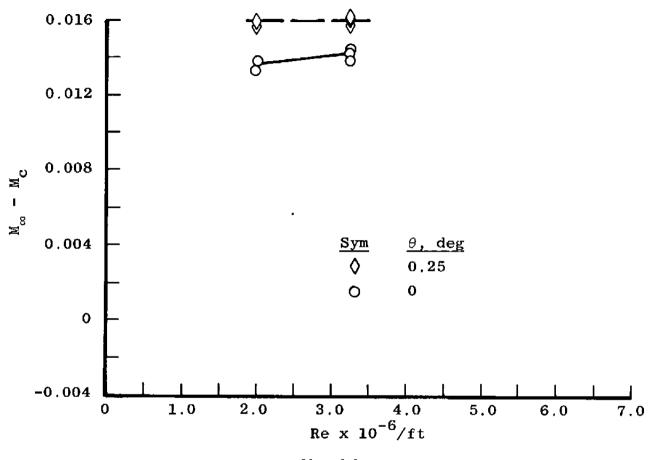
d. $M_\infty = 1.0$
Figure 36. Continued.
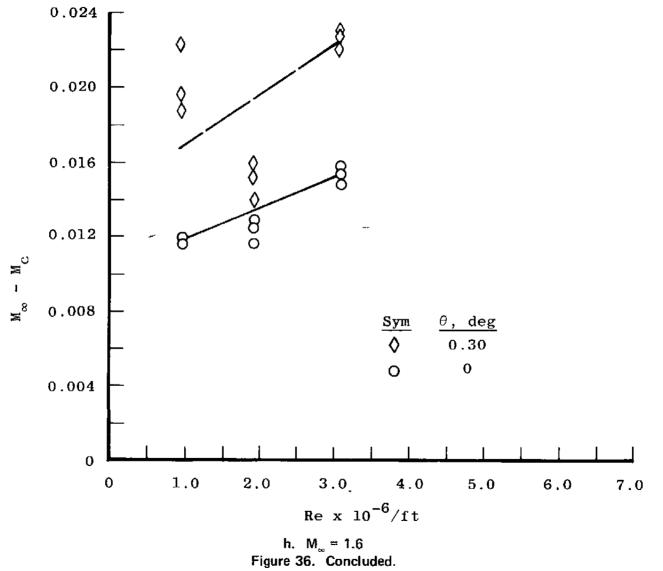
e. $M_\infty = 1.1$

Figure 36. Continued.

f. $M_\infty = 1.2$

Figure 36. Continued.

g. $M_\infty = 1.4$
Figure 36. Continued.

h. $M_\infty = 1.6$
Figure 36. Concluded.
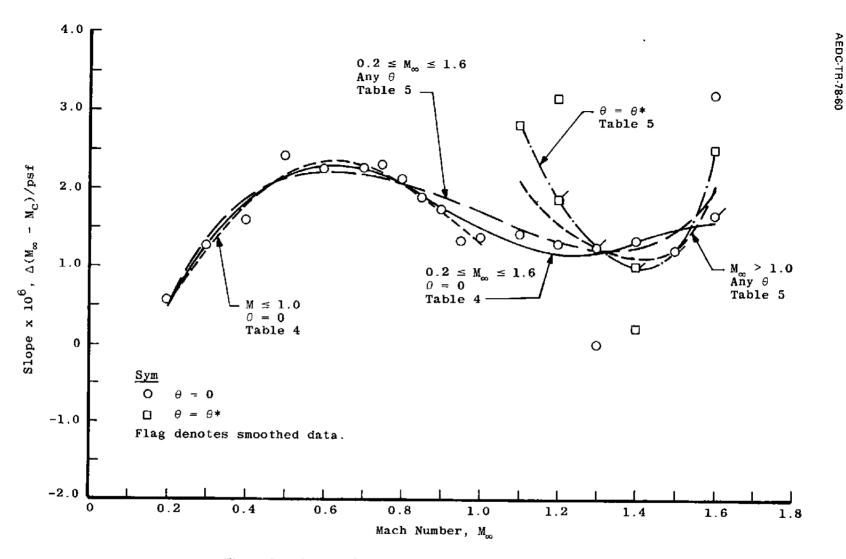
Figure 37. Slopes of Reynolds number correction curves.

Table 1. Coefficients of the Tunnel 16T Mach Number Calibration Curve Fit for $\theta = 0$ and $P_t = 1,600$ psfa

i	$0.2 \le M_\infty \le 1.6$ A_i	$M \le 1.0$ A_i	$M > 1.0$ A_i
0	-9.3949-03	-5.0862-03	7.4395-01
1	9.0218-02	4.9023-02	-2.3868-00
2	-1.9302-01	-5.6043-02	2.8925-00
3	2.2295-01	2.4991-02	-1.5411-00
4	-1.2400-01	----	3.0495-01
5	2.6142-02	----	----
Maximum Residual	0.0017	0.0010	0.0018
Maximum Residual for 95-percent Data	0.0008	0.0007	0.0012

These data apply where the curve is of the form

$$\left(M_\infty - M_c \right)_{P_t=1,600} = \sum_{i=0}^{i=max} A_i \, M_c^i$$

163

Table 2. Coefficients of the Tunnel 16T Mach Number Calibration Surface Fit for Variable Test Section Wall angle and P_t = 1,600 psfa

i	j	$0.2 \le M_\infty \le 1.6$ A_{ij}	$M_\infty \le 1.0$ A_{ij}	$M_\infty > 1.0$ A_{ij}
0	0	-9.8584-03	-4.9906-03	-2.3895-01
1	0	9.5880-02	4.7565-02	5.8313-01
0	1	6.6908-03	8.3066-04	1.2688-01
2	0	-2.1393-01	-5.1577-02	-4.4539-01
1	1	-8.0230-02	-1.0990-02	-2.2367-01
0	2	2.3804-03	2.7874-03	6.1841-02
3	0	2.5547-01	2.1634-02	1.1296-01
2	1	2.1264-01	1.5884-02	1.0232-01
1	2	-3.9646-03	-5.0986-03	-6.1124-02
0	3	2.5358-02	7.9795-04	1.0387-02
4	0	-1.4635-01		
3	1	-1.9698-01		
2	2	2.5858-02		
1	3	-4.9067-02		
0	4	1.0486-03		
5	0	3.1732-02		
4	1	6.3205-02		
3	2	-2.0805-02		
2	3	2.9458-02		
1	4	-3.0575-02		
0	5	-2.6753-02		
Maximum Residual		0.0018	0.0011	0.0017
Maximum Residual for 95-percent Data		0.0011	0.0008	0.0014

These data apply where the surface is of the form

$$\left(M_\infty - M_c \right)_{P_t=1,600} = \sum_{i,j=0}^{i,j=max} A_{ij} M_c^i \theta^j$$

164

Table 3. Coefficients of the Tunnel 16T Mach Number Calibration (Test Entry 1)
for Specific Mach Numbers at Various Reynolds Numbers with $\theta = \theta *$

M_∞	θ, deg	A_o	A_1	A_2
0.55	0	4.6000−03	2.1500−06	0
0.60	0	4.2882−03	2.9701−06	−1.7994−10
0.70	0	4.5274−03	3.3735−06	−2.3264−10
0.80	0	5.7467−03	2.7189−06	−1.7546−10
0.85	0	7.6299−03	1.2622−06	1.0491−10
0.90	0	8.4514−03	9.2368−07	1.5377−10
0.95	0	8.5542−03	1.3185−06	0
1.00	0	8.6345−03	1.4738−06	0
1.10	−0.75	−2.1770−03	5.6597−07	0
1.20	−0.20	8.2328−03	1.8122−06	0
1.30	0.15	1.4600−02	0	0
1.40	0.25	1.3346−02	8.8903−07	0
1.50	0.30	1.8000−02	−3.0000−06	0

These data apply where the curve is of the form

$$M_\infty - M_c = A_o + A_1\,(P_t) + A_2\,(P_t)^2$$

Table 4. Coefficients of the Slopes for the Tunnel 16T Reynolds Number
Corrections with $\theta = 0$

	$0.2 \leq M_\infty \leq 1.6$	$M \leq 1.0$	$M > 1.0$
i	A_i	A_i	A_i
0	$-9.6680-07$	$-2.9466-08$	$5.1165-05$
1	$5.6780-06$	$-1.4009-06$	$-1.7146-04$
2	$1.7117-05$	$3.1342-05$	$2.2030-04$
3	$-4.7320-05$	$-4.9898-05$	$-1.2500-04$
4	$3.5482-05$	$2.1290-05$	$2.6374-05$
5	$-8.4955-06$	0	0
Maximum Residual	$0.30-06$	$0.24-06$	$0.11-06$

These data apply where the curve is of the form

$$\frac{\Delta(M_\infty - M_c)}{psf} = \sum_{i=0}^{i=5} A_i \left[M_{\infty(P_t=1,600)} \right]^i$$

and the corrected Mach number from $P_t = 1,600$ psfa is

$$M_\infty = M_{\infty(P_t=1,600)} + \frac{\Delta(M_\infty - M_c)}{psf} (P_t - 1,600)$$

where $M_{\infty(P_t=1,600)} = (M_\infty - M_c)_{(P_t=1,600)} + M_c$

Table 5. Coefficients of the Slopes for the Tunnel 16T Reynolds Number Corrections for Variable Test Section Wall Angle

i	$0.2 \leq M_\infty \leq 1.6$ [a] A_i	$M > 1.0$ [a] A_i	$M \geq 1.05$ [b] A_i
0	-3.2233-06	3.6035-04	2.5816-04
1	2.6933-05	-1.0853-03	-7.6535-04
2	-5.1207-05	1.2398-03	8.8016-04
3	4.8693-05	-6.3329-04	-4.6051-04
4	-2.4930-05	1.2180-04	9.1848-05
5	5.4470-06	0	0
Maximum Residual	0.58-06	0.07-06	0.01-06

These data apply where the curve is of the form

$$\frac{\Delta(M_\infty - M_c)}{psf} = \sum_{i=0}^{i=5} A_i \left[M_{\infty(P_t=1,600)} \right]^i$$

and the corrected Mach number from $P_t = 1,600$ psfa is

$$M_\infty = M_{\infty(P_t=1,600)} + \frac{\Delta(M_\infty - M_c)}{psf} (P_t - 1,600)$$

where $M_{\infty(P_t=1,600)} = (M_\infty - M_c)_{(P_t=1,600)} + M_c$

---

[a] For any θ; uses average of slopes for $\theta = 0$ and $\theta = \theta*$ at $M > 1.0$. For $M \leq 1.0$ and any θ use $\theta = 0$ data from Table 4.

[b] Specifically for $\theta = \theta*$ (see Fig. 4).

APPENDIX A

TUNNEL AUXILIARY FLOW AND POWER REQUIREMENTS

Data presented in Figs. 13 through 16 indicate that acceptable Mach number distributions can be obtained for various combinations of pressure ratio and wall suction. An optimum pressure ratio may be defined as that associated with minimum total power requirements and acceptable Mach number distributions. The effect of pressure ratio variation on the auxiliary weight flow requirements is shown in Fig. A-1. The data indicate that reducing pressure ratio (to decrease main drive power) significantly increases the auxiliary weight flow requirements (and therefore the auxiliary power).

Typical effects of pressure ratio variation on total power consumption are illustrated in Fig. A-2. The power factor is the total power divided by the tunnel stagnation pressure. These data have been corrected by removing the power of standby compressors and the power associated with flow bypassed through the Mach number control valve. The data presented in Fig. A-2 indicate that for $M_\infty < 0.75$ and supersonic Mach numbers the minimum power requirements occur at the lowest pressure ratios. For $M_\infty = 0.8$ and 0.9 the pressure ratios for minimum power nearly coincide with the nominal pressure ratios (λ^*). This result is consistent with that reported in Ref. 3. As noted in Section 4.1.6, changing tunnel operating procedures and reducing the pressure ratios at $M_\infty \leqslant 0.75$ provide a power savings of from 3 to 9 percent. The pressure ratio should not be reduced below that shown in Figs. 16 and A-2 at $M_\infty < 0.75$, however, since the Mach number distributions would be adversely affected. At supersonic Mach numbers, lowering the pressure ratio significantly below the nominal pressure ratio schedule (Fig. 3) is not recommended. The limiting factor will generally be sting vibrations caused by interaction between the tunnel terminal shock system and the sting support strut.

The data presented in Figs. 17 through 20 indicate that the effects of wall angle variation on the Mach number distributions can be significant. Acceptable Mach number distributions were obtained, however, at almost all wall angles tested. Typical effects of wall angle variation on the tunnel auxiliary flow and total power requirements are presented in Figs. A-3 and A-4. These data indicate that the auxiliary flow and power requirements generally decrease with wall divergence. The tunnel is routinely run with converged wall angles only when the optimum wall angle schedule is utilized at Mach numbers between 1.00 and 1.25. Wall angles associated with the optimum wall angle schedule are noted in Figs. A-3 and A-4. The data in Fig. A-4 indicate that at $M_\infty = 1.1$. use of the optimum wall angle rather than $\theta = 0$ increases the power requirements by about 11 percent.

The data presented in Figs. 21 through 24 indicate that variation of Reynolds numbers has only a small effect on the Mach number distributions. The effects of Reynolds number variation on the tunnel auxiliary flow and power requirements are illustrated in Figs. A-5 and A-6. The data presented in Fig. A-5 show that, except for $M_\infty = 0.8$, the auxiliary flow requirements increase slightly with increasing Reynolds number. The data presented in Fig. A-6 indicate that below $Re = 2.5 \times 10^{-6}$/ft the tunnel total power factor increases significantly with decreasing Reynolds number. The tunnel main drive power is proportional to stagnation pressure; however, the auxiliary power is not. This accounts for the variations in power factor shown in Fig. A-6.
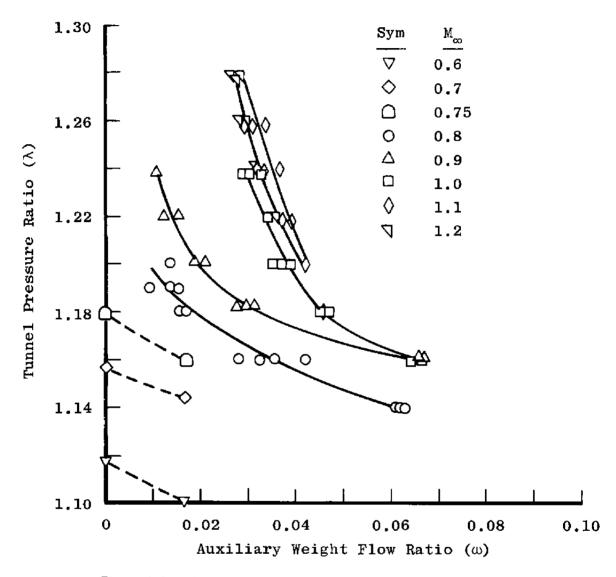
Figure A-1. Effect of pressure ratio variation on auxiliary weight flow
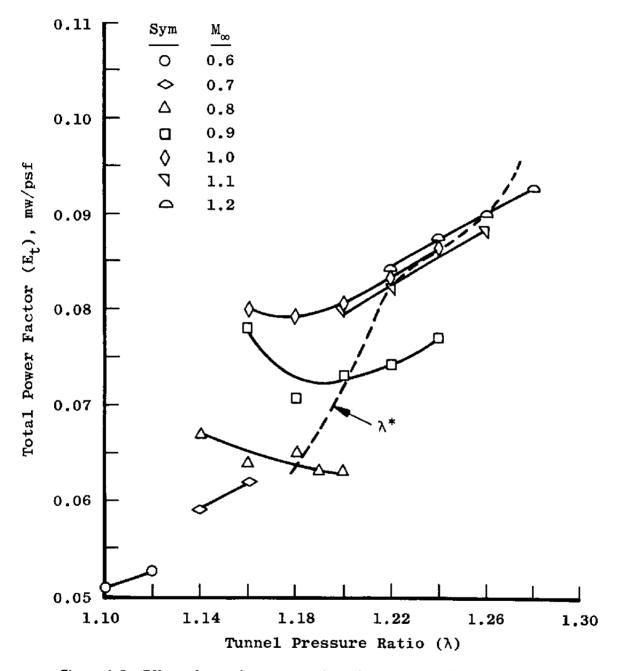requirements with $\theta = 0$ and $P_t = 1,600$ psfa.

Figure A-2. Effect of tunnel pressure ratio variation on the Tunnel 16T total power requirements with $\theta = 0$ and $P_t = 1,600$ psfa.
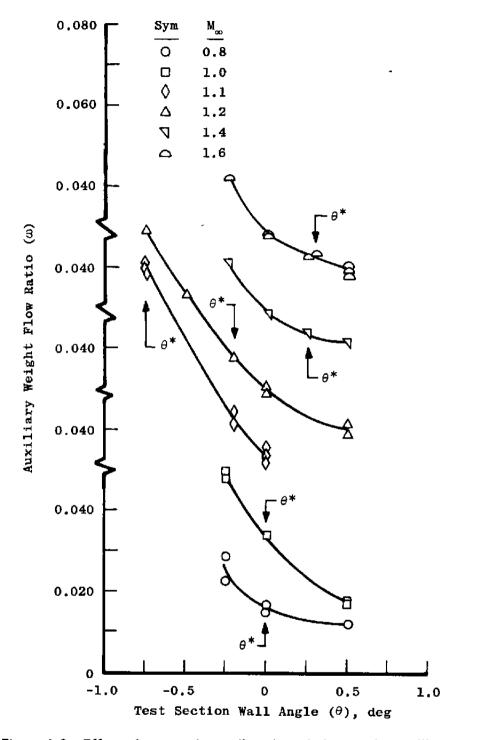
Figure A-3. Effect of test section wall angle variation on the auxiliary weight flow requirements with $\lambda = \lambda^*$ and $P_t = 1,600$ psfa.
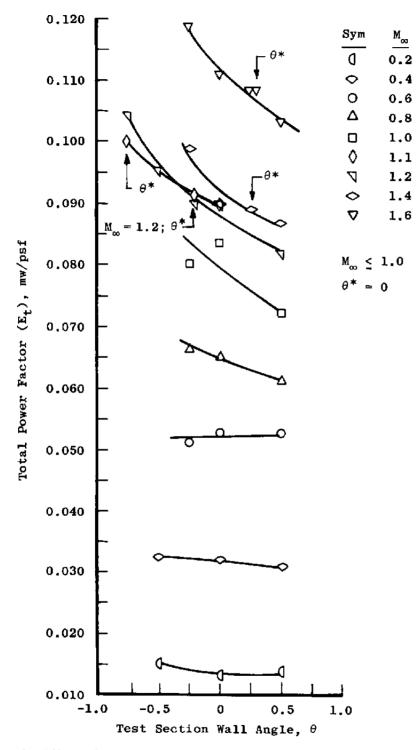
Figure A-4. Effect of test section wall angle variation on Tunnel 16T total power requirements with $\lambda = \lambda^*$ and P_t = 1,600 psfa.
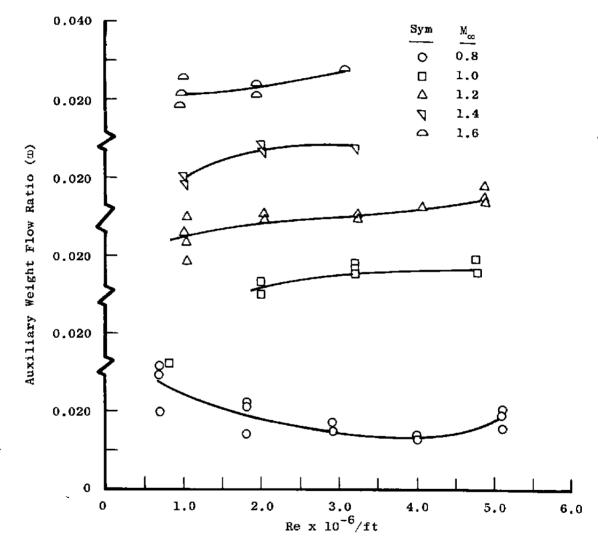
Figure A-5. Effect of Reynolds number variation on the auxiliary weight
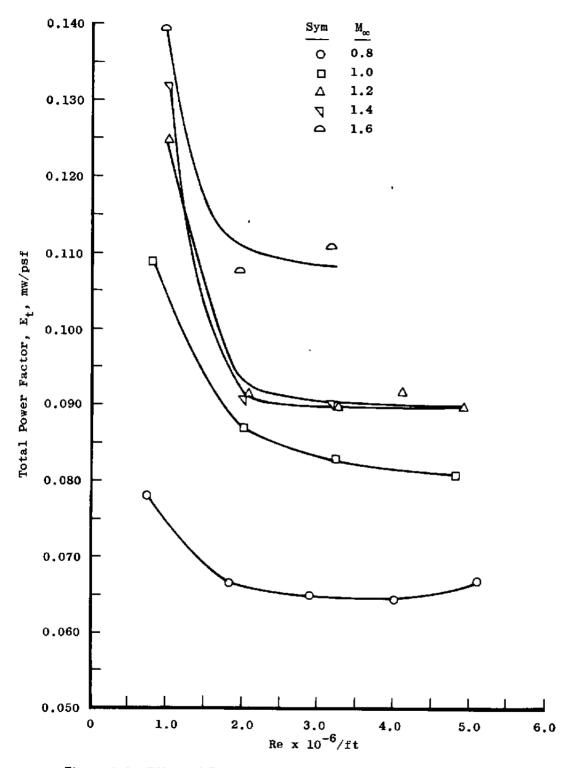flow requirements with $\lambda = \lambda^*$ and $\theta = 0$.

Figure A-6. Effect of Reynolds number variation on tunnel total power
requirements with $\theta = 0$ and $\lambda = \lambda^*$.

NOMENCLATURE

$\bar{C}_p$ Average of local pressure coefficients from tunnel stations 6 to 18

E_t Tunnel total power factor, (total power)/P_t

M   Local Mach number

M_c Equivalent plenum chamber Mach number

M_∞ Free-stream Mach number, determined from the average of local Mach numbers over a specific test region (i.e., tunnel stations 1 to 20, 3 to 19, or 6 to 18.)

P_t Tunnel stagnation pressure, psfa

Re   Unit Reynolds number, 1/ft

θ Test section wall angle, deg (positive when walls are diverged)

θ^* Optimum wall angle, deg (Fig. 4)

λ Tunnel pressure ratio, ratio of P_t to the compressor inlet pressure

λ^* Nominal tunnel pressure ratio (Fig. 3)

σ Standard deviation (conventional statistical parameter)

ω Auxiliary weight flow ratio; auxiliary weight flow divided by tunnel weight flow